Spring 2013

Multiscale modeling and simulation of shock wave propagation

Cory Nelsen
University of Iowa

MULTISCALE MODELING AND SIMULATION OF SHOCK WAVE PROPAGATION

by

Cory Nelsen

A thesis submitted in partial fulfillment
of the requirements for the Master of
Science degree in Mechanical Engineering
in the Graduate College of
The University of Iowa

May 2013

Thesis Supervisor: Associate Professor Shaoping Xiao

Graduate College
The University of Iowa
Iowa City, Iowa

CERTIFICATE OF APPROVAL

_____

MASTER'S THESIS

_____

This is to certify that the Master's thesis of

Cory Nelsen

has been approved by the Examining Committee
for the thesis requirement for the Master of Science
degree in Mechanical Engineering at the May 2013 graduation.

Thesis Committee: _____
Shaoping Xiao, Thesis Supervisor

_____
Hongtao Ding

_____
Albert Ratner

ACKNOWLEDGMENTS

I would like to thank Professor Shaoping Xiao for all of his help and guidance in both this research and my coursework. The knowledge I have gained is invaluable. It has truly been a rewarding and enjoyable experience. I would also like to thank Professors Hongtao Ding and Albert Ratner for taking the time to serve on my thesis committee. In addition, I would like to thank Professor Ding for his time and support over the last year which has been much appreciated.

TABLE OF CONTENTS

LIST OF FIGURES iv

CHAPTER 1 INTRODUCTION 1

1.1 Motivation 1
1.2 Literature Review 2
1.2.1 Multiscale Modeling 2
1.2.2 Flux-Corrected Transport 3

CHAPTER 2 MODEL AND EQUATIONS 5

2.1 Molecular Dynamics 5
2.2 Finite Element Method 6
2.3 Monte Carlo Simulations 9
2.4 Macroscopic Atomistic *Ab Initio* Dynamics 10
2.5 Flux-Corrected Transport 11
2.6 Temperature Related Cauchy-Born Rule 13

CHAPTER 3 MULTISCALE MODELING AT ZERO TEMPERATURE 16

3.1 Shockwave Propagation with MD 16
3.2 Shockwave Propagation with FE 26
3.3 Multiscale Coupling 35

CHAPTER 4 NON-ZERO TEMPERATURE EFFECTS 48

4.1 Monte Carlo Simulation 48
4.2 Shockwave Propagation with TCB Rule 54

CHAPTER 5 SUMMARY AND RECOMMENDATONS 64

5.1 Summary and Conclusions 64
5.2 Future Work 65

REFERENCES 67

LIST OF FIGURES

Figure 3-1: Square shape stress wave propagating along a one-dimensional molecular chain with MD and a spring-model potential. 18

Figure 3-2: Square shape stress wave propagating along a one-dimensional molecular chain with MD and a spring-model potential with FCT applied. 19

Figure 3-3: Decaying stress wave without FCT smoothing in a one-dimensional model with MD and a spring-model potential. 20

Figure 3-4: Decaying stress wave with FCT applied in a one-dimensional molecular chain with MD and a spring-model potential. 20

Figure 3-5: Square shape stress wave propagating along a one-dimensional molecular chain with MD and a LJ potential without FCT applied. 22

Figure 3-6: Square stress wave propagating along a one-dimensional molecular chain with MD and a LJ potential with FCT applied. 22

Figure 3-7: LJ Force as a function of bond length *r*. 23

Figure 3-8: Decaying stress wave without FCT smoothing in a one-dimensional model with MD and a LJ potential. 24

Figure 3-9: Decaying stress wave with FCT smoothing in a one-dimensional model with MD and a LJ potential. 24

Figure 3-10: High magnitude decaying stress wave without FCT smoothing in a one-dimensional model with MD and a LJ potential. 25

Figure 3-11: High magnitude decaying stress wave with FCT smoothing in a one-dimensional model with MD and a LJ potential. 25

Figure 3-12: Square stress wave propagating along a one-dimensional molecular chain with FE and a spring potential without FCT applied. 28

Figure 3-13: Square stress wave propagating along a one-dimensional molecular chain with FE and a spring potential with FCT applied. 28

Figure 3-14: Decaying stress wave without FCT smoothing in a one-dimensional model with FE and a spring potential. 29

Figure 3-15: Decaying stress wave with FCT smoothing in a one-dimensional model with FE and a spring potential. 30

Figure 3-16: Square stress wave propagating along a one-dimensional molecular chain with FE and a LJ potential without FCT applied. 31

Figure 3-17: Square stress wave propagating along a one-dimensional molecular chain with FE and a LJ potential with FCT applied. 32

Figure 3-18: Decaying stress wave without FCT smoothing in a one-dimensional model with FE and a LJ potential. 33

Figure 3-19: Decaying stress wave with FCT smoothing in a one-dimensional model with FE and a LJ potential. 33

Figure 3-20: High magnitude decaying stress wave with FCT smoothing in a one-dimensional model with FE and a LJ potential.....34

Figure 3-21: High magnitude decaying stress wave with FCT smoothing in a one-dimensional model with FE and a LJ potential.....35

Figure 3-22: Square stress wave propagating along a one-dimensional molecular chain with a multiscale model and a spring potential without FCT applied.....37

Figure 3-23: Square stress wave propagating along a one-dimensional molecular chain with a multiscale model and a spring potential with FCT applied.....38

Figure 3-24: Square stress wave propagating along a one-dimensional molecular chain with a multiscale model and a LJ potential without FCT applied.....39

Figure 3-25: Square stress wave propagating along a one-dimensional molecular chain with a multiscale model and a LJ potential with FCT applied.....39

Figure 3-26: Example of transition region elements.....40

Figure 3-27: Square stress wave propagating along a one-dimensional molecular chain with a multiscale model with a transition region and a spring potential without FCT applied. 41

Figure 3-28: Square stress wave propagating along a one-dimensional molecular chain with a multiscale model with a transition region and a spring potential with FCT applied. 41

Figure 3-29: Decaying stress wave propagating along a one-dimensional molecular chain with a multiscale model with a transition region and a spring potential without FCT applied. 42

Figure 3-30: Decaying stress wave propagating along a one-dimensional molecular chain with a multiscale model with a transition region and a spring potential with FCT applied. 43

Figure 3-31: Square stress wave propagating along a one-dimensional molecular chain with a multiscale model with a transition region and a LJ potential without FCT applied. 44

Figure 3-32: Square stress wave propagating along a one-dimensional molecular chain with a multiscale model with a transition region and a LJ potential with FCT applied. 44

Figure 3-33: Low magnitude decaying stress wave propagating along a one-dimensional molecular chain with a multiscale model with a transition region and a LJ potential without FCT applied. 46

Figure 3-34: Low magnitude decaying stress wave propagating along a one-dimensional molecular chain with a multiscale model with a transition region and a LJ potential with FCT applied. 46

Figure 3-35: High magnitude decaying stress wave propagating along a one-dimensional molecular chain with a multiscale model with a transition region and a LJ potential with FCT applied. 47

Figure 3-36: High magnitude decaying stress wave propagating along a one-dimensional molecular chain with a multiscale model with a transition region and a LJ potential with FCT applied. 47

Figure 4-1: MC free energy results for T = 300 K. 49

Figure 4-2: Comparison of free energy from MC simulation and derived potential functions at 300 K. 51

Figure 4-3: Comparison of free energy from MC simulation and approximation potential gradients at 300 K. 51

Figure 4-4: MC free energy results for T = 200 K. 52

Figure 4-5: Comparison of free energy from MC simulations at different temperatures. 53

Figure 4-6: Comparison of free energy from MC simulation and derived potential functions at 200 K. 53

Figure 4-7: Comparison of free energy from MC simulation and approximation potential gradients at 200 K. 54

Figure 4-8: Comparison of wave propagation with TCB and derived potential. 55

Figure 4-9: Square stress wave at zero temperature without FCT. 56

Figure 4-10: Square stress wave at zero temperature with FCT. 57

Figure 4-11: Decaying stress wave at zero temperature without FCT. 57

Figure 4-12: Decaying stress wave at zero temperature with FCT. 58

Figure 4-13: Square stress wave at 300 K without FCT. 59

Figure 4-14: Square stress wave at 300 K with FCT. 59

Figure 4-15: Decaying stress wave at 300 K without FCT. 60

Figure 4-16: Decaying stress wave at 300 K with FCT. 60

Figure 4-17: Wave speed comparison for temperatures of 0 K and 300 K. 61

Figure 4-18: Square stress wave at 200 K without FCT. 62

Figure 4-19: Square stress wave at 200 K with FCT. 62

Figure 4-20: Decaying stress wave at 200 K without FCT.....63
Figure 4-21: Decaying stress wave at 200 K with FCT.....63

CHAPTER 1

INTRODUCTION

1.1 Motivation

Shockwaves, like other waves, carry energy and propagate through a medium. The propagation is governed by a second order differential equation, which is hyperbolic in nature, and therefore the propagation occurs with a finite speed (Mariani, 2009). They are characterized by a nearly discontinuous change in characteristics of the medium, with an extremely rapid rise in pressure, temperature, and density across the shock front. This rapid change can cause deformation, fracture and fragmentation, polymorphic phase changes, and other alterations which can cause failure to occur in materials (Davison, 2008). Researchers are interested in studying the potentially destructive effects of shockwaves both for applications where it is desired, such as military explosions and ballistic impacts, and resistances, such as supersonic flow and military defense.

Experimental studies can be very costly, both in time and material. Therefore, it is preferred to use numerical simulations, whose only major cost is computation time. The simulation of nanoscale mechanics is of growing interest as the area of nanotechnology expands. Unfortunately, there are limitations to the size of nanoscale simulations due to limits in computational power and time. Multiscale models and simulations have been of growing interest in the area of computational nanotechnology because they can overcome these size limitations (Xiao, 2006).

Multiscale models allow the study of multiple scales for a problem, such as quantum or atomic levels to macroscopic and continuum levels. This is important because different physical laws may be used to govern the physics at different scales. For example, in fluid dynamics, Molecular Dynamics and Newton's Laws govern the motion of individual atoms at the nanoscale, while at the macroscale the Navier-Stokes equations are obeyed. While multiscale problems have been studied for a long time mathematically,

technology is now evolving to a point where the mathematics can begin to be studied and used in applied sciences, such as nanotechnology (E, 2003).

Because of the nearly discontinuous nature of shockwaves, oscillations are generated behind the shock fronts, which are numerical errors that develop during the simulation. A common technique to remove these oscillations is applying artificial viscosity to the system (Kawai, 2007). While effective at reducing the oscillations, this method spreads the shock fronts over several elements and dissipates the total energy in the system. Alternatively, the flux-corrected transport method has been shown to remove oscillations without causing these problems, and a finite element with flux-corrected transport (FCT) method for the study of shock wave propagation was proposed by Shaoping Xiao (Xiao, 2004).

The main goal of this thesis is to develop and conduct multiscale modeling and simulation of shockwave propagation with the removal of numerical errors and inclusion of temperature effects. The first chapter of this thesis presents the motivation and relevant background information for the study. Chapter 2 provides the mathematical models and governing equations used. The study of FCT on multiscale models and non-zero temperatures are discussed in Chapters 3 and 4. Finally, a summary of the results and a recommendation for future work is given in Chapter 5.

1.2 Literature Review

1.2.1 Multiscale Modeling

Traditionally, engineering models focus on a single scale. If a problem is a macroscale application, then continuum models are used and any information about the smaller scales can be found from constitutive relationships. Similarly, if the problem is a microscopic application, then it is assumed that any process is homogenous at the macroscopic scales. Therefore, there has been a disconnect between the two scales, where the study and analysis of one scale require little knowledge of the other.

As technology becomes more advanced, the problems studied for practical application become more complex, and the simple constitutive equations become inadequate. On the other side, any problem could theoretically be modeled using quantum theory, or another molecular based method such as molecular dynamics. The problem with this is that the theories are too complex or too small in dimension to be applied to practical problems. It is this problem that multiscale modeling seeks to remedy.

By modeling different scales simultaneously, the efficiency and size dimensions of the macroscale can be combined with the accuracy and effectiveness of the molecular scales. Multiscale modeling has been studied historically by mathematics, but the use for practical problems has been developed more recently. The first types of problems studied with multiscale modeling were problems involving chemical reactions, where quantum theory was used in the reaction region, and more classical models were used in the rest of the model. As researchers have realized that this method can be useful in all applications, not just chemistry or material science, and numerical computations have become more efficient, multiscale modeling has become of much greater interest and a rapidly expanding research area (E, 2011).

1.2.2 Flux-Corrected Transport

When simulating discontinuous phenomena, there is often a high level of error due to the generation of non-physical oscillations behind the shock fronts. This occurs because standard simulation techniques assume a continuous interpolation between the data points. Because these oscillations are solely numerical errors, they need to be removed if more accurate results are desired from the simulation (Mariani, 2009).

Traditionally these oscillations were removed by applying an artificial viscosity to the model. There have also been methods developed that focus on the time integration to remove the oscillations, such as the α-method (Hilber, 1977). The problem with these methods was that while the oscillations were damped out, new non-physical effects were

introduced. The energy of the system was steadily dissipated, and the shock fronts became less sharp and spread over several elements or grids.

The flux-corrected transport method was developed as a way to remove the oscillations without introducing these other non-physical effects, keeping the shock fronts sharp and discontinuous. It is a post-processing method that is composed of two steps, the first being the transport stage, and the second being the antidiffusive or corrective stage (Boris, 1973). The errors introduced in the transport stage are removed by the corrective stage by handling and analyzing the diffusive and antidiffusive fluxes. While the method was originally used with fluid dynamics and finite-difference methods, it has been expanded to the well-developed finite element methods and stress-waves in solids (Xiao, 2004).

CHAPTER 2

MODEL AND EQUATIONS

In this thesis, the simulation of shockwave propagation in multiscale models at a zero or finite temperature field is studied, in order to examine the effectiveness of an algorithm which reduces the oscillations generated due to the discontinuous nature of the wave. In this chapter, the governing equations for the various methods and algorithms used are detailed.

2.1 Molecular Dynamics

Molecular Dynamics (MD) is a powerful tool that is used to elucidate many physical phenomena at the nanoscale. It assumes that the motion of the particles (molecules) in the system obey the laws of classical mechanics. In a MD simulation, the system is first initialized by selecting initial positions and velocities for each particle. Once initialization is done, the forces are calculated for each particle, and positions and velocities are updated through time integration of Newton's equations of motion, shown in equation 2.1, where *u* is the

Equation 2.1: MD equation of motion

$$\ddot{u} = \frac{f_{ext} + f_{int}}{m}$$

displacement, the superposed dots represent material time derivatives, f_{ext} is the externally applied force, f_{int} is the internal force, and *m* is the particle mass. The internal force is derived from the potential energy equation as shown in equation 2.2, where *U* is the potential, and *r* is the distance between neighboring particles. Equation 2.2 is solved repeatedly until the target time of the simulation is reached, at which point the desired quantities of the simulation are measured or recorded. MD simulations are considered

Equation 2.2: Internal force equation

$$f_{int} = -\frac{\partial U}{\partial r}$$

excellent approximations for many materials (Frenkel, 1996).

MD simulations can be used to measure various material and thermal properties of a system over time. For example, individual particles do not have a defined temperature, which is instead described by the kinetic energy of the system as shown in equation 2.3, where K is the average kinetic energy, k_b is the Boltzmann Constant, and T is the temperature. Thus, the instantaneous temperature will fluctuate as the particle velocities change, and an initial temperature for the system could be given by prescribing initial velocities to each particle following a Boltzmann distribution, while keeping the mean velocity zero, so that the center of mass is stationary.

Equation 2.3: Instantaneous temperature relative to average kinetic energy

$$K = \frac{1}{2} k_b T$$

2.2 Finite Element Method

Finite element methods are numerical techniques used to find approximate solutions to systems which are mathematically governed by partial differential equations. They have been widely developed and commonly used to find solutions to complex problems. In general, the problem domain is discretized into elements, and the PDEs are solved along the boundary with either an algebraic system of equations (steady state problems) or a system of ordinary differential equations (transient problems). The governing equations and discretization for the finite element method are detailed below.

The motion of a given domain Ω from its reference configuration Ω_0 can be described by equation 2.4, where **x** is the spatial (Eulerian) coordinates, **X** is the material

(Lagrangian) coordinates, and *t* is time. The momentum equations for the reference configuration can then be written as equation 2.5, where **P** is the nominal stress tensor, **b**

Equation 2.4: Mapped equation of motion

$$\mathbf{x} = \Phi(\mathbf{X}, t)$$

Equation 2.5: Momentum equation for reference domain configuration

$$\nabla_0 \cdot \mathbf{P} + \rho_0 \mathbf{b} = \rho_0 \ddot{\mathbf{u}}, \qquad \sum_j \frac{\partial P_{ji}}{\partial X_j} + \rho_0 b_i = \rho_0 \ddot{u}_i$$

is the body force, and ρ_0 is the initial density. However, if the current configuration is equivalent to the reference configuration, then equation 2.5 can instead be written in the (identical) spatial form as in equation 2.6, where ρ is the current density. Equation 2.7 can

Equation 2.6: Momentum equation for current domain configuration

$$\nabla_0 \cdot \boldsymbol{\sigma} + \rho \mathbf{b} = \rho \ddot{\mathbf{u}}, \qquad \sum_j \frac{\partial \sigma_{ji}}{\partial x_j} + \rho b_i = \rho \ddot{u}_i$$

Equation 2.7: Conservation of mass

$$\rho J = \rho_0$$

then be derived from the conservation of mass, where *J* is the Jacobian determinant of the deformation gradient **F**, as defined in equation 2.8. Using the total Lagrangian finite element method, the displacements in the Lagrangian mesh can be approximated by

Equation 2.8: Jacobian and deformation gradient

$$J = \det(\mathbf{F}), \qquad \mathbf{F} = \frac{\partial x_i}{\partial X_i}$$

equation 2.9, where $N_J(\mathbf{X})$ is the shape function of the material coordinates in the total Lagrangian description. The approximation of the first derivatives of displacement can then be written as equation 2.10. Equation 2.11, then, shows the Galerkin weak form of the conservation of linear momentum equation, where δu_i is the test function and $\bar{t}_i$ is the

Equation 2.9: Approximate displacements in Lagrangian mesh

$$\mathbf{u}^h(\mathbf{X},t) = \mathbf{N}^{\mathrm{T}}(\mathbf{X})\mathbf{u}(t), \qquad u_i^h(\mathbf{X},t) = \sum_J N_J(\mathbf{X})u_{iJ}(t)$$

Equation 2.10: Approximate first derivative of displacement

$$\nabla_0\mathbf{u}^h(\mathbf{X},t) = \mathbf{B}^{\mathrm{T}}(\mathbf{X})\mathbf{u}(t), \qquad \frac{\partial u_i^h(\mathbf{X},t)}{\partial X_j} = \sum_J \frac{\partial N_J(\mathbf{X})}{\partial X_j}u_{iJ}(t)$$

Equation 2.11: Conservation of momentum in weak form

$$\int_{\Omega_0} \delta u_i \rho_0 \ddot{u}_i \,\mathrm{d}\Omega_0 = \int_{\Omega_0} \delta u_i \rho_0 b_i \,\mathrm{d}\Omega_0 - \int_{\Omega_0} \sum_j \frac{\partial(\delta u_i)}{\partial X_j} P_{ji} \,\mathrm{d}\Omega_0 + \int_{\Gamma_0^t} \delta u_i \bar{t}_i \,\mathrm{d}\Gamma_0^t$$

boundary traction. Equation 2.1, the equation of motion, can then be rewritten for a node *I* as equation 2.12, where the external force f_{iI}^{ext} and internal force f_{iI}^{int} are given by equations 2.13 and 2.14, respectively.

Equation 2.12: FE equation of motion for node *I*

$$M_I\ddot{u}_{iI} = f_{iI}^{ext} - f_{iI}^{int}$$

Equation 2.13: External nodal force

$$f_{iI}^{ext} = \int_{\Omega_0} \rho_0 N_I(\mathbf{X}) b_i \,\mathrm{d}\Omega_0 + \int_{\Gamma_0^t} N_I(\mathbf{X})\bar{t}_i \,\mathrm{d}\Gamma_0^t$$

Equation 2.14: Internal nodal force

$$f_{iI}^{int} = \int_{\Omega_0} \sum_j \frac{\partial N_I(\mathbf{X})}{\partial X_j} P_{ji} \, \mathrm{d}\Omega_0$$

2.3 Monte Carlo Simulations

Monte Carlo (MC) simulations use a classical statistical approach and the importance sampling to determine the properties of a system. It can be used on a variety of different ensembles, depending on which properties are kept constant, and the free energy of the system. Most MC methods can be reduced to stages: select a particle at random and calculate its energy in the current state, give the particle a random displacement and calculate its new energy, and finally accept or reject the displacement based on the change in energy.

The probability is based on a Boltzmann distribution, shown in equation 2.15, where P_i is the probability of a system to be in state i with energy E_i. This probability is

Equation 2.15: Boltzmann distribution probability

$$P_i = \frac{\exp(-E_i/k_bT)}{\sum_j \exp(-E_j/k_bT)}$$

related to the partition function Q, equation 2.16, which is the sum over all quantum states i of the Boltzmann factor $\exp(-E_i/k_bT)$, where $\mathbf{r}^N$ represents the coordinates of all N particles, and the function E is the energy of the system. The Helmholtz free energy can then be written as equation 2.17. Using equation 2.15, the probabilities of the system being at the current state **m** ($P_\mathbf{m}$), and a trial state **n** ($P_\mathbf{n}$) are calculated, and the probability of the trial move occurring from **m** to **n**, $A_{\mathbf{mn}}$, is found from equation 2.18. Thus, the

Equation 2.16: Partition function

$$Q = \int \exp\left(-\frac{E(\mathbf{r}^N)}{k_bT}\right) d\mathbf{r}^N$$

Equation 2.17: Helmholtz free energy

$$F_H = -\frac{1}{k_b T} \ln Q$$

Equation 2.18: Trial move probability

$$A_{\mathbf{mn}} = \frac{P_{\mathbf{n}}}{P_{\mathbf{m}}} = \left[\frac{\exp(-\beta E_{\mathbf{n}})}{Q}\right] \Big/ \left[\frac{\exp(-\beta E_{\mathbf{m}})}{Q}\right], \qquad \beta = \frac{1}{k_b T}$$

partition function does not necessarily need to be computed every time. It can be seen that the change in energy can be directly compared, so equation 2.18 can be rewritten as equation 2.19. Therefore, if $\delta E_{\mathbf{mn}}$ is greater than zero, the probability $A_{\mathbf{mn}}$ is calculated

Equation 2.19: Reduced trial move probability

$$A_{\mathbf{mn}} = \exp(-\beta \delta E_{\mathbf{mn}}), \qquad \delta E_{\mathbf{mn}} = E_{\mathbf{n}} - E_{\mathbf{m}}$$

to determine if the trial move occurs, and if $\delta E_{\mathbf{mn}}$ is less than zero, $A_{\mathbf{mn}}$ is set to 1, and the trial move occurs.

2.4 Macroscopic Atomistic *Ab Initio* Dynamics

Macroscopic Atomistic *Ab Initio* Dynamics (MAAD) is a concurrent multiscale coupling method, used to couple the different length scales used in multiscale modeling. It can be used for length scales from the atomic level to the macroscopic level (Lu, 2005). MAAD is based on the conservation of energy in the system using the total Hamiltonian as shown in equation 2.20, where *H* represents the Hamiltonian for the designated

Equation 2.20: Total Hamiltonian of MAAD system

$$H_{tot} = H_{FE} + H_{MD} + H_{TB} + H_{FE/MD} + H_{MD/TB}$$

subscript, with FE/MD and MD/TB representing the finite element/molecular dynamics handshake region and the molecular dynamics/tight-bonding quantum level handshake region, respectively. In the FE/MD handshake region, the MD particles are constrained to align with the FE nodes.

The first three terms of equation 2.20 are the Hamiltonians for the regions where only one length scale is used, as defined by equation 2.21, where U_i is the strain or

Equation 2.21: Single domain Hamiltonian

$$H_i = U_i + K_i$$

potential energy of domain i, and K_i is the kinetic energy. The Hamiltonians for the handshake regions are composed equally of the two domains, as shown in equation 2.22.

Equation 2.22: Handshake domain Hamiltonian

$$H_{i/j} = \frac{1}{2}H_i + \frac{1}{2}H_j = \frac{1}{2}(U_i + K_i + U_j + K_j)$$

Similarly, the forces from each region are calculated and applied equally to the handshake domain.

2.5 Flux-Corrected Transport

The flux-corrected transport (FCT) algorithm contains two stages, the transport stage and the antidiffusion stage, where the antidiffusion stage corrects the numerical errors from the transport stage. These two stages allow the FCT algorithm to treat discontinuities without generating oscillations. The FCT algorithm was originally used in finite-difference (FD) methods. The general FCT is composed of six steps outlined below in equations 2.23 through 2.28.

The first step is the transport calculation, where the trial values of any function Q are obtained at time step n+1 and spatial step j with equation 2.23, where Δt is the time-

Equation 2.23: FCT trial values

$$\tilde{Q}_j^{n+1} = f(Q_j^n, \Delta t, \Delta X)$$

step and ΔX is the spatial increment. The second step is equation 2.24, the calculation of

Equation 2.24: FCT diffusive flux

$$\varphi_j^0 = \eta_1\left(Q_{j+1}^n - Q_j^n\right)$$

the diffusive fluxes, where η_1 is the diffusive coefficient. The third step is equation 2.25,

Equation 2.25: FCT diffusion

$$\bar{Q}_j^{n+1} = \tilde{Q}_j^{n+1} + \varphi_j^0 - \varphi_{j-1}^0$$

the diffusion step. Step four is equation 2.26, the calculation of the antidiffusive fluxes,

Equation 2.26: FCT antidiffusive flux

$$\varphi_j^1 = \eta_2\left(\tilde{Q}_{j+1}^n - \tilde{Q}_j^n\right)$$

where η_2 is the antidiffusive coefficient. Step five is equation 2.27, the limitation of

Equation 2.27: FCT limitation of antidiffusive flux

$$\varphi_j^C = S * \max\left\{0, \min\left[S * \Delta_{j-1}, \left|\varphi_j^1\right|, S * \Delta_{j+1}\right]\right\}$$

antidiffusive fluxes, where $S = \text{sign}(\varphi_j^1)$, and $\Delta_{j-1} = \bar{Q}_j^{n+1} - \bar{Q}_{j-1}^{n+1}$. The final step is

equation 2.28, the antidiffusion step.

Equation 2.28: FCT antidiffusion

$$Q_j^{n+1} = \bar{Q}_j^{n+1} - \varphi_j^C + \varphi_{j-1}^C$$

While FCT has been shown to efficiently eliminate oscillations when used with FD methods, it must be applied to each of the several PDEs that are usually needed for FD. For FE methods, the same algorithm can be used by applying the FCT to the velocity. Since each component of velocity is independent, the FCT can be applied to each component separately, provided that a structured mesh is used.

2.6 Temperature Related Cauchy-Born Rule

When larger systems on the nanoscale are to be simulated, various multiscale methods are available to help reduce the required computational time and power. Regardless of what methods are used, a continuum-approximation approach, such as the Cauchy-Born (CB) rule, is used as a homogenization technique (E, 2006). The CB rule assumes locally homogenous deformation in the continuum domain. The atomic potential can then be used in the constitutive equation as the strain energy density (potential energy density) for the continuum via the deformation gradient, as shown in equations 2.29 and 2.30, where **F** is the gradient of deformation and X is the reference (Lagrangian) coordinates in equation 2.29, and in equation 2.30 W_C is the total strain energy, w_c is the strain energy density, and Ω_0 is the reference configuration. The first Piola–Kirchhoff stress, **P**, can then be obtained from equation 2.31. However, it is assumed that the continuum domain

Equation 2.29: Deformation gradient in continuum domain

$$\mathbf{F} = \frac{\partial x}{\partial X}$$

Equation 2.30: Total strain energy

$$W_C = \int_{\Omega_0} w_c(\mathbf{F})\, d\Omega_0$$

Equation 2.31: First Piola-Kirchhoff stress

$$\mathbf{P} = \frac{\partial w_c(\mathbf{F})}{\partial \mathbf{F}}$$

is at zero temperature. The Temperature-Related Cauchy-Born (TCB) rule, however, provides a homogenization technique which allows non-zero temperatures to be used (Xiao, 2006).

There are several ways to include temperature effects. One such way is to use a potential function that includes the entropy due to lattice vibration, such as an Einstein description similar to course graining of vibrations (Najafabadi, 1992). Another technique, which is used in the TCB rule, is a free energy minimization technique (Dupuy, 2005). Instead of the potential energy, the Helmholtz free energy, or effective energy, is used instead. The atomic Helmholtz free energy equation is shown in equation 2.32, where F_H is the Helmholtz free energy, $\bar{h}$ = $h/2\pi$ with h being Planck's constant, n

Equation 2.32: Atomic Helmholtz free energy

$$F_H = U(x) + nk_bT \sum_j \ln\left[2\sinh\left(\frac{\bar{h}D_I^{1/2n}}{2k_bT}\right)\right]$$

is the number of degrees of freedom per atom, and D_I is the determinate of the diagonalized local dynamic matrix, used to calculate the principal frequencies of atom I. The TCB rule assumes that at a given temperature, atoms have the same local vibration, the vibration of an atom is harmonic, and the coupled vibration of atoms is negligible, in

addition to the assumption of locally homogenous deformation from the standard CB rule.

The total free energy can be found with equation 2.33, where W_H is the total free energy and ρ_n is the number of atoms per unit volume. The first Piola-Kirchhoff stress as a function of temperature, therefore, can be found from equation 2.34, where w_H is the free energy density as a function of the deformation gradient and temperature.

Equation 2.33: Total free energy

$$W_H = \int_{\Omega_0} w_c(\mathbf{F})\, d\Omega_0 + nk_b \int_{\Omega_0} \rho_n T \ln\left[\frac{\bar{h}(D(\mathbf{F}))^{1/2n}}{k_b T}\right] d\Omega_0$$

Equation 2.34: Piola-Kirchhoff stress for free energy

$$\mathbf{P}(\mathbf{F}, T) = \frac{\partial w_H(\mathbf{F}, T)}{\partial \mathbf{F}}$$

CHAPTER 3

MULTISCALE MODELING AT ZERO TEMPERATURE

One of the major limiting factors in a MD simulation is the size of the model. In order to have a larger model, many more atoms must be added. However, if a multiscale method is used, the computation time can be drastically reduced. There are two types of multiscale methods: hierarchical multiscale methods and concurrent multiscale methods. Hierarchical models use a consistent time scale while using continuum approximations to approach the nanoscale. In this thesis, shock wave propagation in a molecule chain is studied. In this chapter, the concurrent MAAD method is used to couple the MD domain with the FE domain. The effects of the FCT algorithm are first studied on MD and FE methods independently in sections 3.1 and 3.2, respectively, while section 3.3 investigates the effects of the coupled multiscale model.

3.1 Shockwave Propagation with MD

Whenever MD is used for simulations, the potential function must first be chosen to describe interaction between two neighboring molecules in the simulated molecule chain. Two potential functions will be studied here, the first being a simple spring model shown in equation 3.1, where k is the spring stiffness, r_0 is the unstretched bond length, and r is

Equation 3.1: Spring potential function

$$U_s = \frac{1}{2}k(r_0 - r)^2$$

the current bond length. The second potential function examined is the Lennard-Jones 6-12 (LJ) potential, shown in equation 3.2, where ε is the depth of the energy well. The simulation will be done with a one-dimensional model, with the assumption that a

Equation 3.2: LJ potential function

$$U_{LJ} = 4\varepsilon\left[\frac{1}{4}\left(\frac{r_0}{r}\right)^{12} - \frac{1}{2}\left(\frac{r_0}{r}\right)^{6}\right]$$

particle only interacts with its immediate neighbors. The flowchart for the MD simulation can be written as follows:

1) Initialization and initial conditions: give initial positions to the particles in equilibrium position.
2) Calculate particle forces as in equation 2.2.
3) Obtain particle velocities: $\tilde{v}_i^{n+1} = v_i^n + \left(f_i^{ext} + f_i^{int}\right)/m_i\,\Delta t$. If FCT is not being used, $v_i^{n+1} = \tilde{v}_i^{n+1}$ and go to (4), otherwise apply FCT to velocity:
    a) Calculate diffusive fluxes: $\varphi_i^0 = \eta_1(v_{i+1}^n - v_i^n)$.
    b) Diffusion: $\bar{v}_i^{n+1} = \tilde{v}_i^{n+1} + \varphi_i^0 - \varphi_{i-1}^0$.
    c) Calculate antidiffusive fluxes: $\varphi_i^1 = \eta_2(\tilde{v}_{i+1}^n - \tilde{v}_i^n)$.
    d) Apply limitation of antidiffusive fluxes:
    $\varphi_i^C = S * \max\{0, \min[S * \Delta_{i-1}, |\varphi_i^1|, S * \Delta_{i+1}]\}$,
    where $S = \text{sign}(\varphi_i^1)$, and $\Delta_{i-1} = \bar{v}_i^{n+1} - \bar{v}_{i-1}^{n+1}$.
    e) Antidiffusion: $v_i^{n+1} = \bar{v}_i^{n+1} - \varphi_i^C + \varphi_{i-1}^C$.
4) Update the positions and apply any boundary conditions: $u_i^{n+1} = u_i^n + v_i^{n+1}\Delta t$.
5) Output if simulation is complete; if not, return to (2).

An external force will applied to the end of the molecular chain. The boundary condition for the other end can be fixed at zero displacement, or can be a free end.

The first potential function considered is the spring-model. Thus, the total force on a particle *i* is calculated as in equation 3.3. A square stress wave is considered with the spring-model parameters $k = 100$ N/m and $r_0 = 0.01$ nm. A force with magnitude 30 nN is applied to a molecular chain with a free end for 1.3 seconds and then released. A single particle has a mass of 0.1 kg. A free end

Equation 3.3: Total particle force from spring potential

$$f_i^{tot} = f_i^{ext} + k[u_{i+1} - 2u_i + u_{i-1}]$$

boundary condition is used for the opposite end of the chain. Figures 3-1 and 3-2 show the wave at three different times: $t_1 = 1.6$, $t_2 = 5.5$, and $t_3 = 10.3$ s. Figure 3-1 shows the oscillations being generated behind the shock fronts without any filtering, while a very good discontinuous wave profile can be seen in Figure 3-2 when the FCT algorithm is applied.

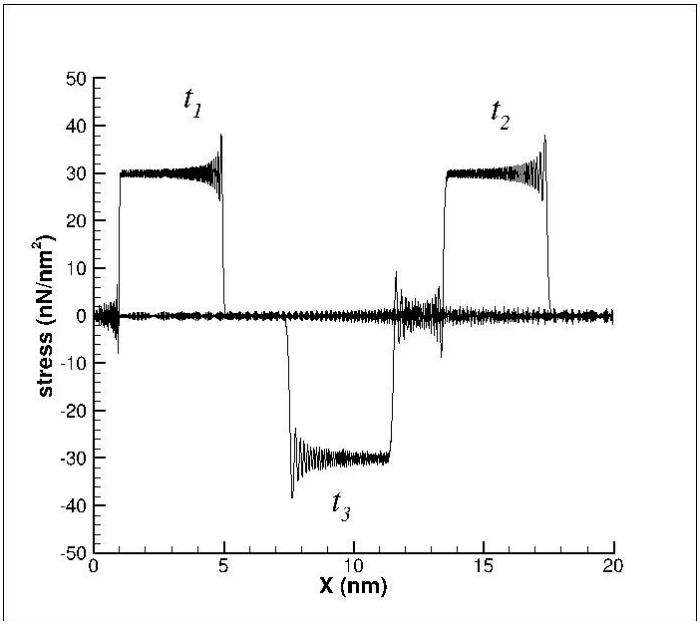

Figure 3-1: Square shape stress wave propagating along a one-dimensional molecular chain with MD and a spring-model potential.

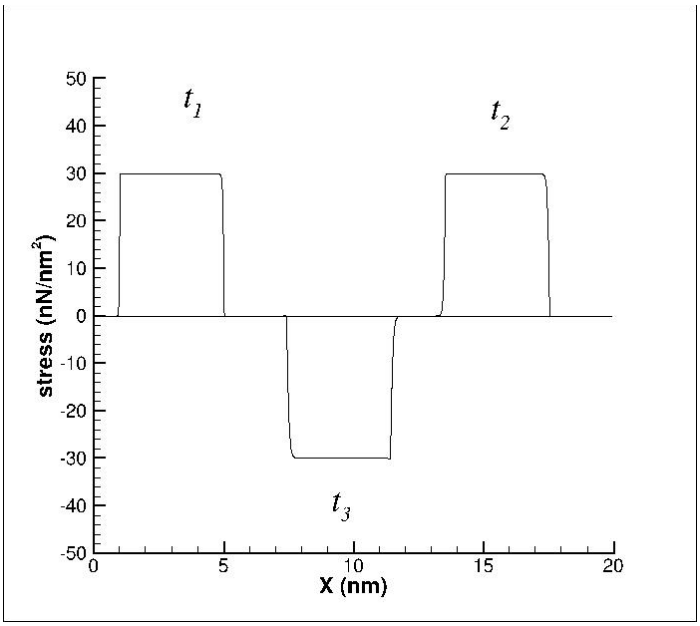

Figure 3-2: Square shape stress wave propagating along a one-dimensional molecular chain with MD and a spring-model potential with FCT applied.

Next, a different wave shape is examined by changing the applied load and keeping all other properties constant. Instead of a constant magnitude, the load exponentially decays after the initial application. Figures 3-3 and 3-4 show the wave without FCT applied and with FCT applied, respectively. It can be seen that the algorithm can remove the oscillations while preserving the discontinuous wave front and the peak of the wave. It should be noted that in both cases the wave perfectly retains its shape as it propagates through the system. This is due to the spring-model potential being very simple, and its derivative, which is the internal force, being linear. Because the slope for the internal force is constant, it does not matter how high or low the stress is, the stiffness is always the same, and thus the front (loading) wave and back (unloading) wave always have the same speed, even if the stresses are at different magnitudes.

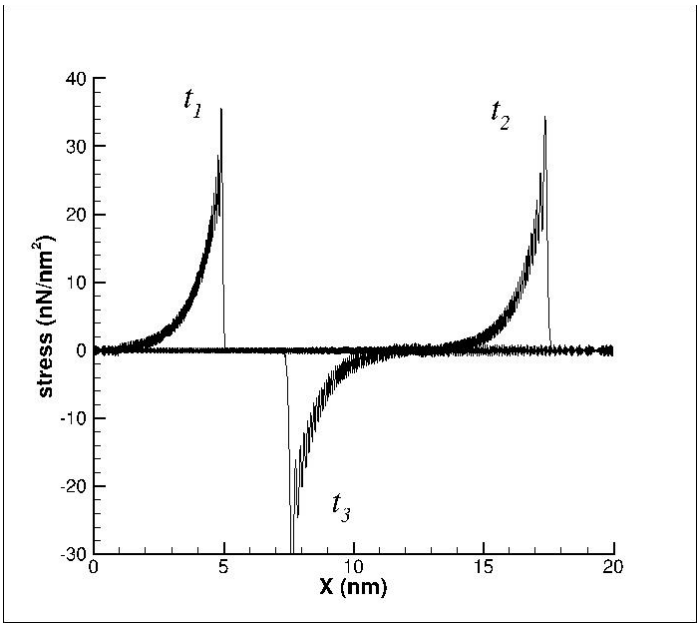

Figure 3-3: Decaying stress wave without FCT smoothing in a one-dimensional model with MD and a spring-model potential.

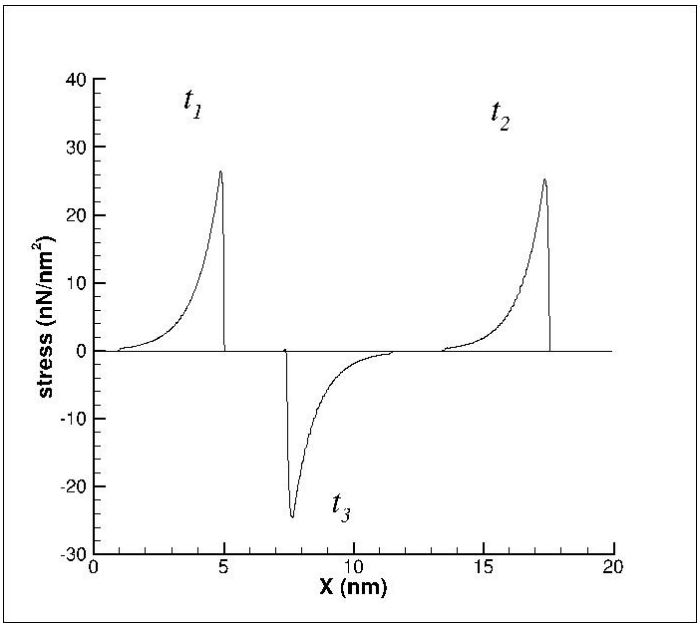

Figure 3-4: Decaying stress wave with FCT applied in a one-dimensional molecular chain with MD and a spring-model potential.

Next, the more complex LJ potential is used, with $\varepsilon = 10$ nJ and $r_0 = 0.01$ nm. The total force on particle *i* when the LJ potential is used can be written as equation 3.4.

Equation 3.4: Total particle force from LJ potential

$$f_i^{tot} = f_i^{ext} + 12\frac{\varepsilon}{r_0}\left[\left(\frac{r_0}{u_i - u_{i-1}}\right)^7 - \left(\frac{r_0}{u_i - u_{i-1}}\right)^{13} - \left(\frac{r_0}{u_{i+1} - u_i}\right)^7 + \left(\frac{r_0}{u_{i+1} - u_i}\right)^{13}\right]$$

As with the spring-model potential, a square stress wave will be examined first. A force of 30 nN is applied to the end of the molecular chain for 0.004 s. Figures 3-5 and 3-6 show the wave without filtering and with the FCT algorithm, respectively, at times $t_1 = 0.0075$, $t_2 = 0.0175$, and $t_3 = 0.035$ s. It can be seen that oscillations are again generated behind the shock fronts, and that the FCT algorithm effectively removes the oscillations while keeping a sharp, discontinuous wave profile. Also, because the stress is small enough here, the equivalent stiffness due to the LJ potential is almost a constant. Therefore, the loading and unloading waves have nearly the same (and constant) speed, so the shape is almost perfectly maintained. However, as will be discussed below, when using the LJ potential the wave speed for different stress levels will vary, because the equivalent stiffness (second derivative of the potential) is not constant. Higher stresses will cause slower wave speeds, so the loading wave will begin to slope backwards, while the unloading wave will become more vertical. This phenomenon will be examined more closely by studying the decaying wave below.

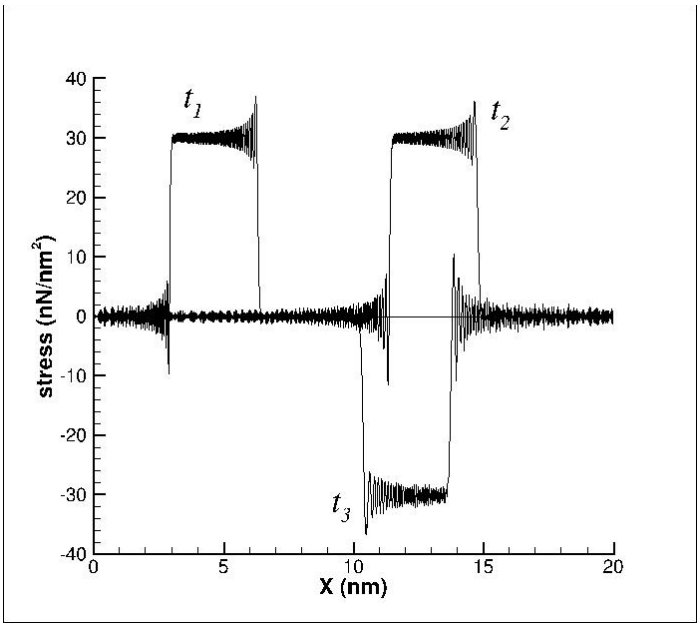

Figure 3-5: Square shape stress wave propagating along a one-dimensional molecular chain with MD and a LJ potential without FCT applied.

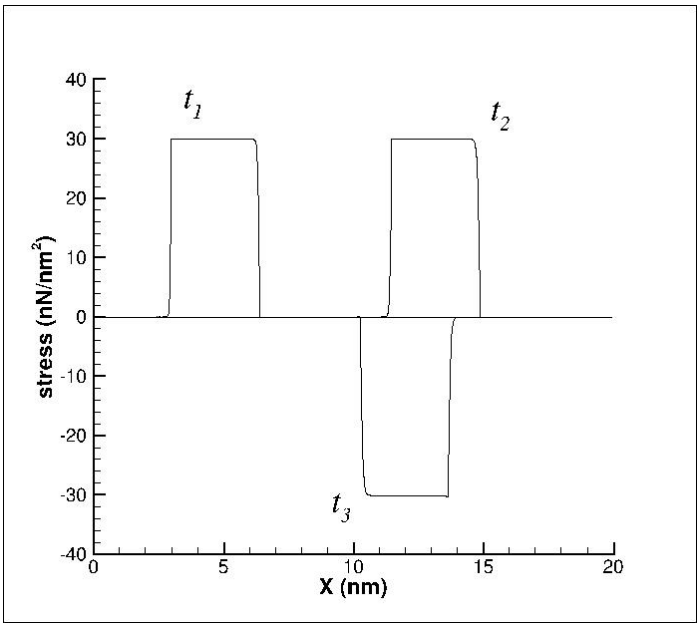

Figure 3-6: Square stress wave propagating along a one-dimensional molecular chain with MD and a LJ potential with FCT applied.

Next, a wave similar to the exponentially decaying wave is studied, but the initial magnitude is held for 0.002 s, and then decays for 0.003 s down to zero. As shown in Figure 3-7, the internal force is nonlinear, so the stiffness is not constant but instead depends on the bond length, and therefore the stress level, at that position. Because the unloading wave has a lower stress magnitude, it travels faster than the loading wave. As the unloading wave catches the loading wave, the plateau begins to shrink, and the loading wave begins to slope back towards the unloading wave, as shown in Figures 3-8 through 3-11. In Figures 3-8 and 3-9, the initial loading magnitude is 30 nN, while in Figures 3-10 and 3-11 the loading magnitude is ten times greater at 300 nN. It can be seen that because the higher stresses cause greater bond lengths, the difference in speed between the loading and unloading waves is also greater, so the plateau shrinks more rapidly. It can also be seen that the FCT algorithm effectively removes the oscillations and generates a good discontinuous front without altering this property in any way, and allows the shrinking plateau effect to be more easily observed.

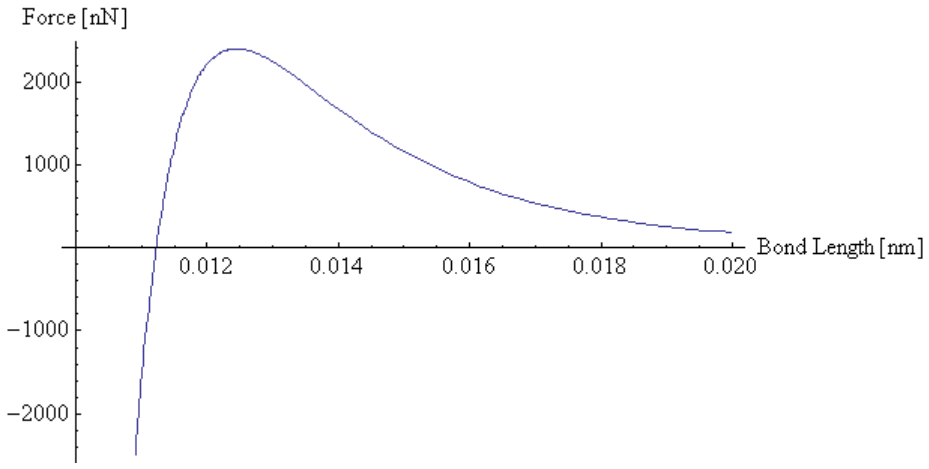

Figure 3-7: LJ Force as a function of bond length *r*.

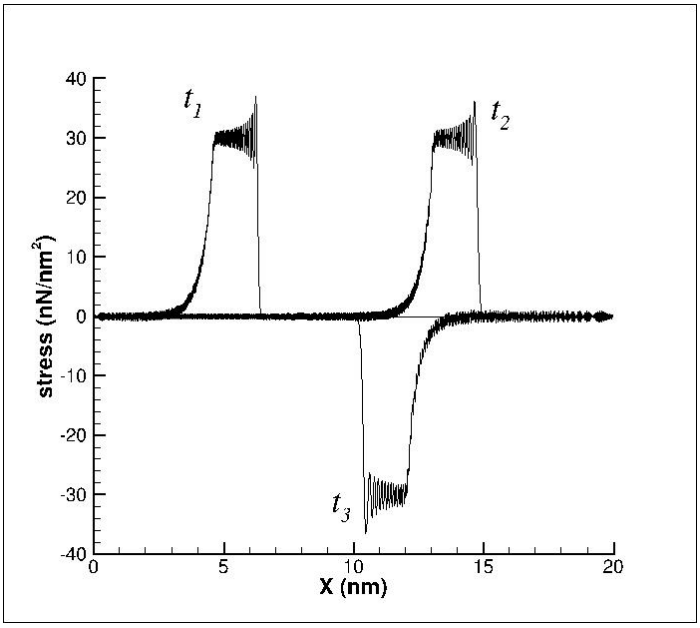

Figure 3-8: Decaying stress wave without FCT smoothing in a one-dimensional model with MD and a LJ potential.

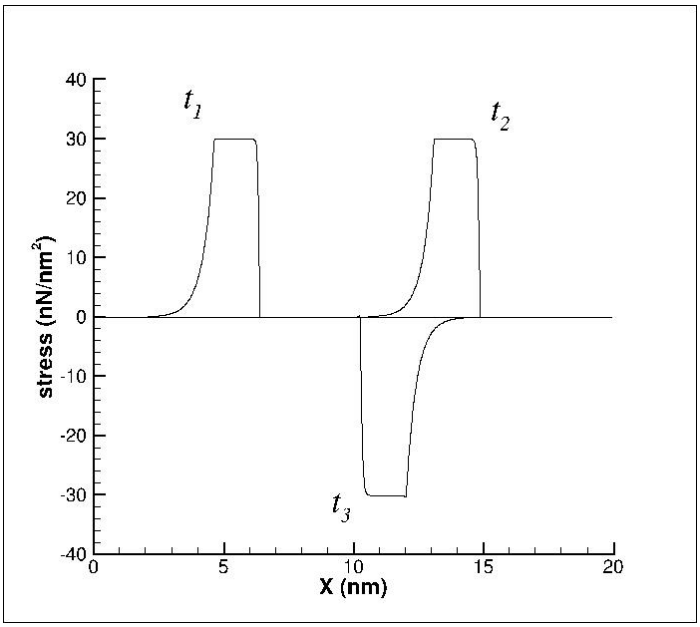

Figure 3-9: Decaying stress wave with FCT smoothing in a one-dimensional model with MD and a LJ potential.

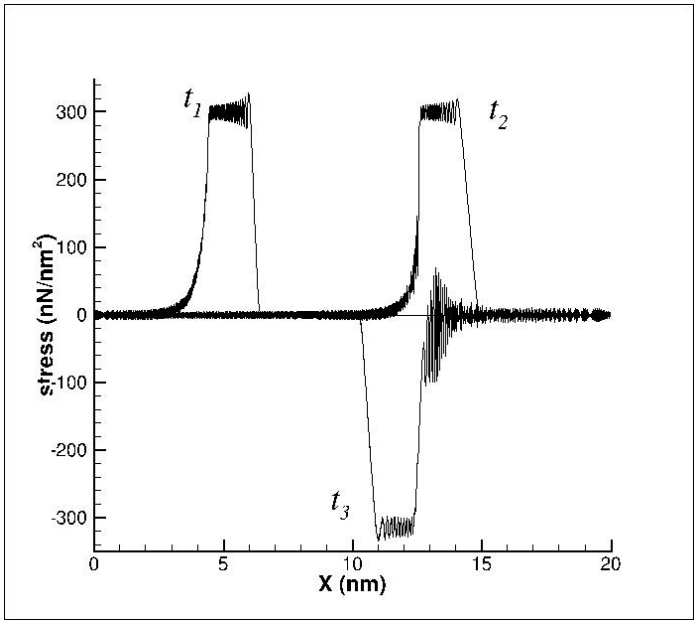

Figure 3-10: High magnitude decaying stress wave without FCT smoothing in a one-dimensional model with MD and a LJ potential.

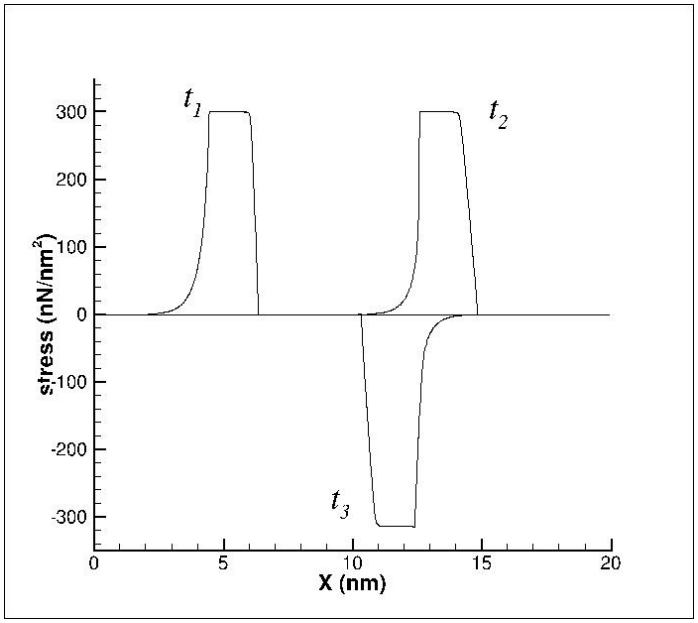

Figure 3-11: High magnitude decaying stress wave with FCT smoothing in a one-dimensional model with MD and a LJ potential.

3.2 Shockwave Propagation with FE

In order to capture the nanoscale properties of a system while using FE methods, a homogenization technique must be used. In this case, the Cauchy-Born rule for a nanoscale-continuum approximation will be used. It is assumed that within an element the deformation is homogenous. The deformation gradient is then used to calculate the strain energy from equation 2.30, which depends on the potential function used for the nanoscale. For a spring potential, the energy density can be written as equation 3.5, where l_0 and l are the undeformed and deformed lengths of the FE element, respectively. The

Equation 3.5: Energy density for spring potential

$$w_c = \frac{U}{r_0} = \frac{kr_0}{2}(\mathbf{F}-\mathbf{1})^2, \qquad \mathbf{F} = \frac{r}{r_0} = \frac{l}{l_0}$$

first Piola-Kirchhoff (PK) stress can then be found from equation 2.31, as shown in equation 3.6. Once the PK stress has been found, the internal forces can be calculated from

Equation 3.6: First PK stress for spring potential

$$\mathbf{P} = \frac{\partial w_c(\mathbf{F})}{\partial \mathbf{F}} = k * r_0 * (\mathbf{F}-1)$$

equation 2.14. Using a linear interpolation, the internal forces for a one-dimensional model is equivalent the first PK stress, as shown in equation 3.7 where f_1^{int} is the internal

Equation 3.7: Internal nodal force for one-dimensional model

$$f^{int} = \begin{bmatrix} f_1^{int} \\ f_2^{int} \end{bmatrix} = \int_0^{L_0} \begin{bmatrix} \frac{\partial}{\partial x}\left(\frac{-x}{L_0}\right) \\ \frac{\partial}{\partial x}\left(\frac{x}{L_0}\right) \end{bmatrix} * \mathbf{P}\, \mathrm{d}L_0 = \begin{bmatrix} -\mathbf{P} \\ +\mathbf{P} \end{bmatrix}$$

force on the first node of an element, and f_2^{int} is the internal force on the second node of the element. Thus, for a system using the spring potential, the total force on a node *i* can be calculated from equation 3.8.

Equation 3.8: Total force on FE node *i*

$$f_i^{tot} = f_i^{ext} + \frac{k * r_0}{l_0}(u_{i+1} - 2u_i + u_{i-1})$$

The square wave will again be the first case studied using a FE approximation for the spring potential MD model used in the previous section, with $k = 100$ N/m, $r_0 = 0.01$ nm, and l_0 representing five bonds: $l_0 = 0.05$ nm. An external force of 30 nN is applied to the left end of the molecular chain for 1.3 s and then released. Figures 3-12 and 3-13 show the wave at times $t_1 = 1.6$, $t_2 = 5.5$, and $t_3 = 10.3$ s. The oscillations generated behind the shock fronts can be seen in Figure 3-12. While the oscillations are more course than in the MD model, it can be seen that the wave has the same magnitude, length, shape, and position as the MD model with the same conditions and parameters in Figure 3-5. While the wave in Figure 3-12 appears to becoming more course as it propagates, it can be seen that the FCT filtering corrects this degradation, and keeps a sharp discontinuous profile.

Next, the exponentially decaying wave using the spring potential will be examined, using the same parameters and bond/element lengths, with the difference being that 0.65 s after the load is applied, it exponentially decays down to zero. As shown

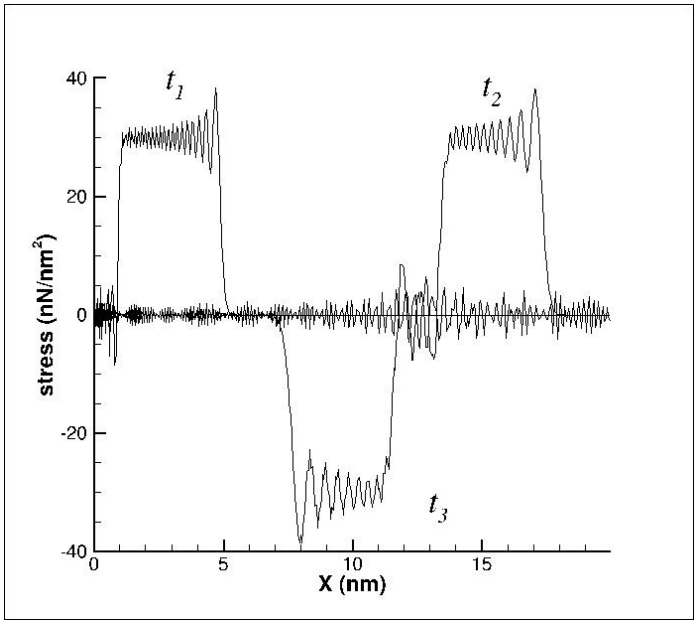

Figure 3-12: Square stress wave propagating along a one-dimensional molecular chain with FE and a spring potential without FCT applied.

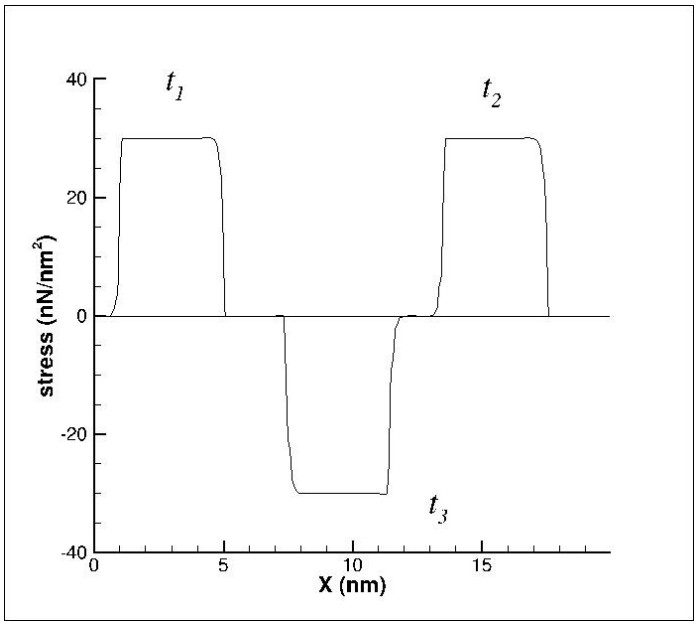

Figure 3-13: Square stress wave propagating along a one-dimensional molecular chain with FE and a spring potential with FCT applied.

in Figure 3-14, the wave without FCT filtering is much more course than the MD model, and this coarseness causes the wave to start breaking down as it propagates. However, the FCT smoothing both removes the oscillations and restores the integrity of the wave profile, as shown in Figure 3-15. It should be noted for both the square wave and the exponentially decaying wave, the wave speed is constant regardless of stress level because the strain energy density was derived from a spring potential function for the nanoscale, and that any decomposition of the wave is instead due to the how course the model is compared to the size of the wave.

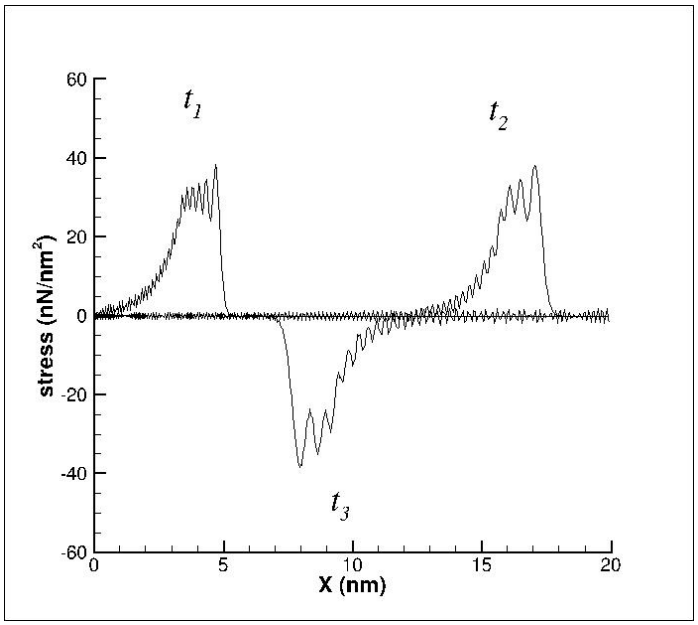

Figure 3-14: Decaying stress wave without FCT smoothing in a one-dimensional model with FE and a spring potential.

Next, the FE model with the strain energy density derived from the LJ potential will be investigated. The energy density when using the LJ potential can be written as equation 3.9, and therefore the first Piola-Kirchhoff stress for the LJ potential can be written as equation 3.10. From the PK stress, the total force on a node *i* can then be

written as equation 3.11. It can be seen that because the LJ potential is a function of the ratio r_0/r, which is simply the inverse of the defined deformation gradient, that the PK stress and total force equations do not change very much from the MD model to the FE model when there is only one degree of freedom.

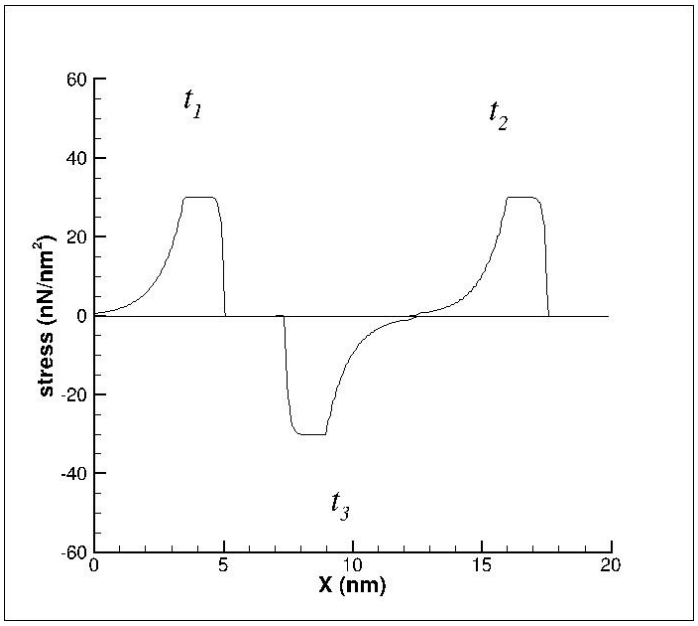

Figure 3-15: Decaying stress wave with FCT smoothing in a one-dimensional model with FE and a spring potential.

Equation 3.9: Energy density for LJ potential

$$w_c = \frac{4\varepsilon}{r_0}\left(\frac{1}{4}\left(\frac{1}{F}\right)^{12} - \frac{1}{2}\left(\frac{1}{F}\right)^{6}\right), \qquad F = \frac{r}{r_0} = \frac{l}{l_0}$$

Equation 3.10: First PK stress from LJ potential

$$w_c = \frac{12\varepsilon}{r_0}\left(\left(\frac{1}{F}\right)^{7} - \left(\frac{1}{F}\right)^{13}\right), \qquad F = \frac{r}{r_0} = \frac{l}{l_0}$$

Equation 3.11: Total force on node *i* from LJ nanoscale potential

$$f_i^{tot} = f_i^{ext} + 12\frac{\varepsilon}{r_0}\left[\left(\frac{l_0}{u_i - u_{i-1}}\right)^7 - \left(\frac{l_0}{u_i - u_{i-1}}\right)^{13} - \left(\frac{l_0}{u_{i+1} - u_i}\right)^7 + \left(\frac{l_0}{u_{i+1} - u_i}\right)^{13}\right]$$

Once the internal forces can be determined, the stress waves can be analyzed. Using similar parameters to the MD model, $\varepsilon = 10$ nJ, $r_0 = 0.01$ nm, and $l_0 = 0.05$ nm, a force of magnitude 30 nN is applied for 0.004 s and then released. Figures 3-16 and 3-17 show the wave before and after the FCT was applied, respectively, at times $t_1 = 0.0075$, $t_2 = 0.0175$, and $t_3 = 0.035$ s. Similar to the FE model with the spring potential, it can be seen that in Figure 3-16 the wave is slowly breaking down due to how course the model is, and the FCT again restores the wave while removing the oscillations generated behind the shock fronts. Also, when the FCT is applied, the stress level is constant across the wave, so both the loading and the unloading wave have

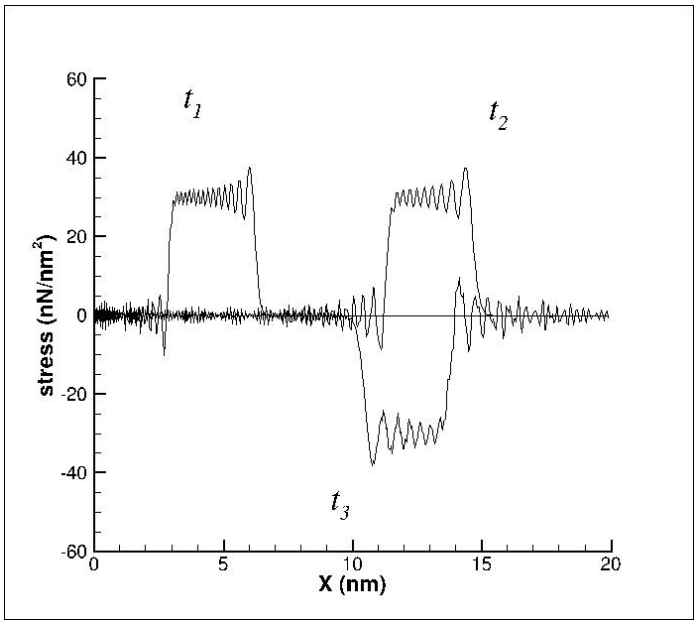

Figure 3-16: Square stress wave propagating along a one-dimensional molecular chain with FE and a LJ potential without FCT applied.

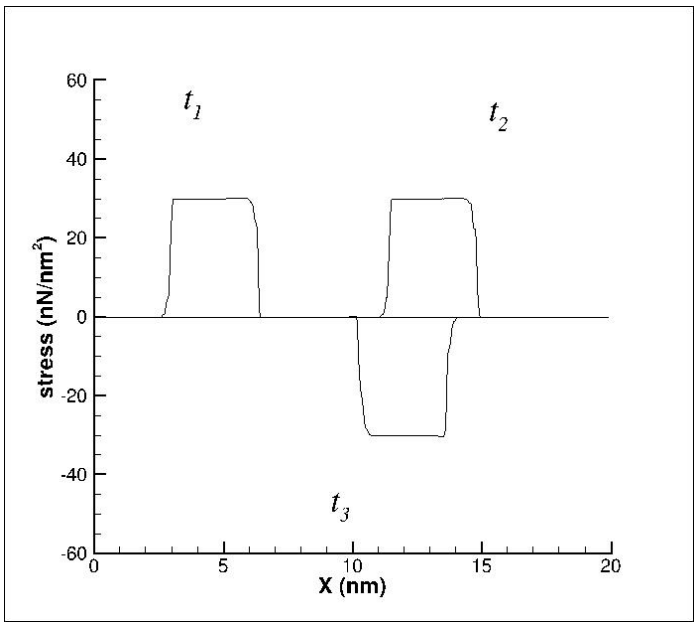

Figure 3-17: Square stress wave propagating along a one-dimensional molecular chain with FE and a LJ potential with FCT applied.

the same speed, and therefore there is little to no change in shape, size, or magnitude as the wave propagates.

For the exponentially decaying wave, the same parameters and model are used with the only difference again being that after the initial magnitude is held for 0.002 s, it decays exponentially down to zero. The decaying wave with an initial magnitude of 30 nN is shown in Figures 3-18 and 3-19, before and after applying the FCT, respectively, at times $t_1 = 0.0075$, $t_2 = 0.0175$, and $t_3 = 0.035$ s. It can be seen that the effects of both the coarseness of the model and the changing stiffness of the bonds are present. However, with the low magnitude, only one of the effects is easily visible at a time. In Figure 3-18, the decomposition of the wave due to how course the model is makes it difficult to see the sloping of the loading wave and shrinking plateau. Once the FCT is applied, however, the coarseness effect is eliminated, and the effect of the unloading wave traveling faster than the loading wave can be more easily observed. As with the MD

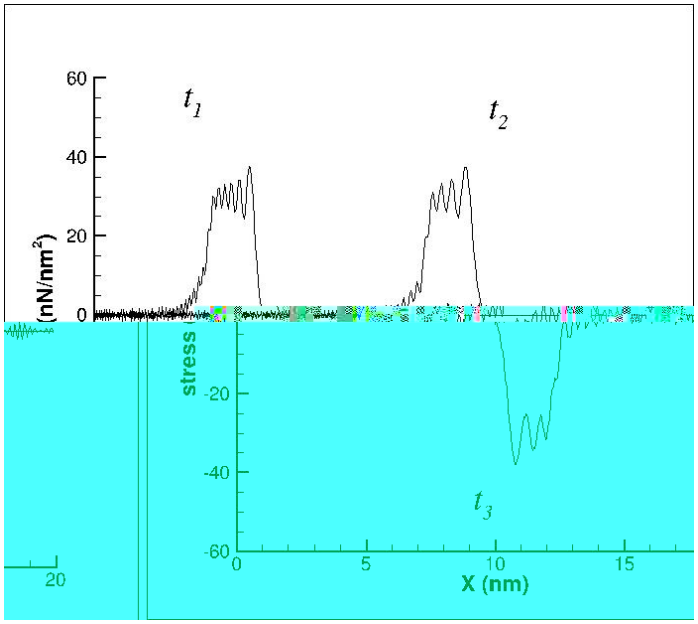

Figure 3-18: Decaying stress wave without FCT smoothing in a one-dimensional model with FE and a LJ potential.

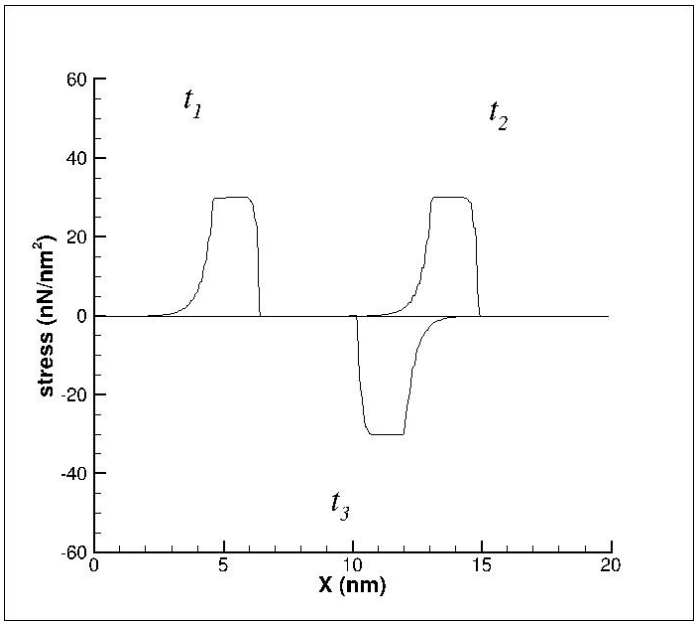

Figure 3-19: Decaying stress wave with FCT smoothing in a one-dimensional model with FE and a LJ potential.

model, a higher magnitude of stress causes a larger change in stiffness to occur, which results in the speed difference between the loading wave and unloading wave to be amplified. In Figures 3-20 and 3-21, the initial magnitude of the applied force is increased to 300 nN. With the larger magnitude, it becomes more obvious that the loading wave is sloping back even without the FCT being applied, as seen in Figure 3-20. It can also be seen by comparing Figure 3-21 and 3-19 that with the higher magnitude force, the difference in speed between the loading wave and unloading is much greater, just as in the MD model. It can also be seen that, like the FE model derived from the spring potential, the FE models from the LJ potential have the same wave speed, shape, and magnitude as in the MD model with the same conditions. This is expected, as the FE model is used to approximate the MD model while reducing computation time and energy.

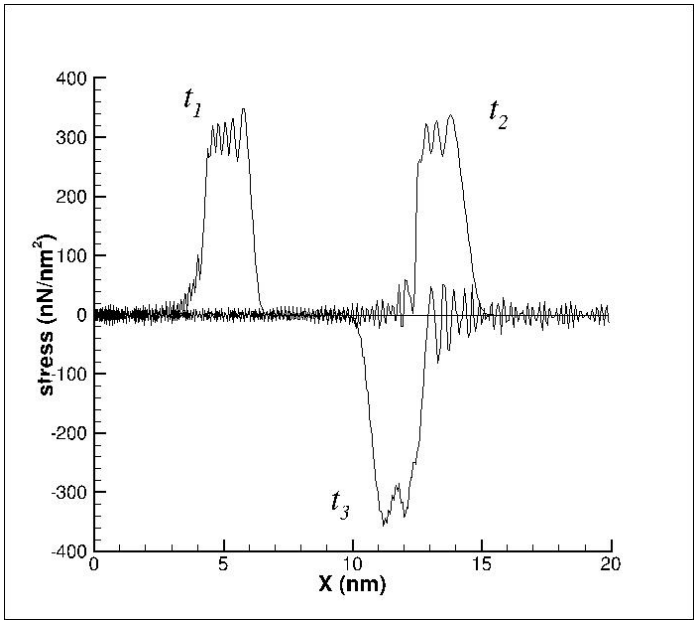

Figure 3-20: High magnitude decaying stress wave with FCT smoothing in a one-dimensional model with FE and a LJ potential.

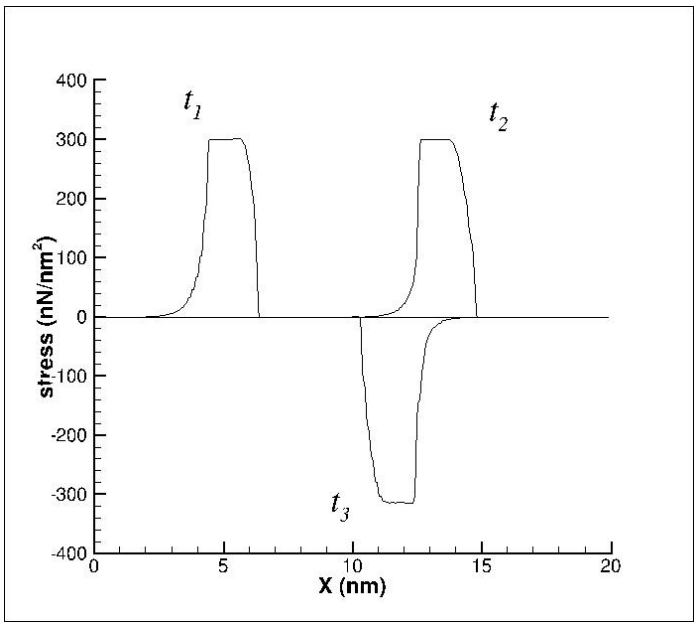

Figure 3-21: High magnitude decaying stress wave with FCT smoothing in a one-dimensional model with FE and a LJ potential.

3.3 Multiscale Coupling

In sections 3.1 and 3.2 it was shown that the FCT algorithm can effectively remove oscillations generated in the simulation while keeping sharp, discontinuous wave profiles intact, even if the wave began to break down in the course FE model when the FCT algorithm was not applied. In this section, the MD and FE domains will be coupled together using the MAAD method. Therefore, the MD and FE contribute equally to the internal forces in the handshake region. For a one-dimensional problem, this can be modeled using a single node or particle. Therefore, one side is represented by the MD domain, and the other is represented by the FE domain, and the MD particle at the interface is also constrained as a FE node. The mass of this center particle is then contributed equally from the MD and FE domains, as shown in equation 3.12.

First, the direct coupling of the two domains will be examined, where the handshake domain goes directly from the MD bonds to the full FE length with no

Equation 3.12: MAAD handshake particle mass

$$M_{hs} = \frac{1}{2} * m + \frac{1}{2}\frac{l_0}{r_0} * m = \frac{m}{2}\left(1 + \frac{l_0}{r_0}\right)$$

transition. Using a spring potential, the total force on the handshake particle *i* can be written as equation 3.13. Using the parameters $k = 100$ N/m, $r_0 = 0.01$ nm, and l_0 representing five bonds: $l_0 = 0.05$ nm, a square wave is examined by applying an external force of 30 nN to the left end of the molecular chain for 1.3 s and then released. Figure 3-22 shows the wave at times $t_1 = 1.6$, $t_2 = 5.5$, and $t_3 = 10.3$ s. By comparing Figure 3-22 to

Equation 3.13: Total force on handshake particle from spring potential

$$f_i^{tot} = k\left[r_0 - u_i + u_{i-1} + \frac{r_0}{l_0}\left(\frac{u_{i+1} - u_i}{l_0} - 1\right)\right]$$

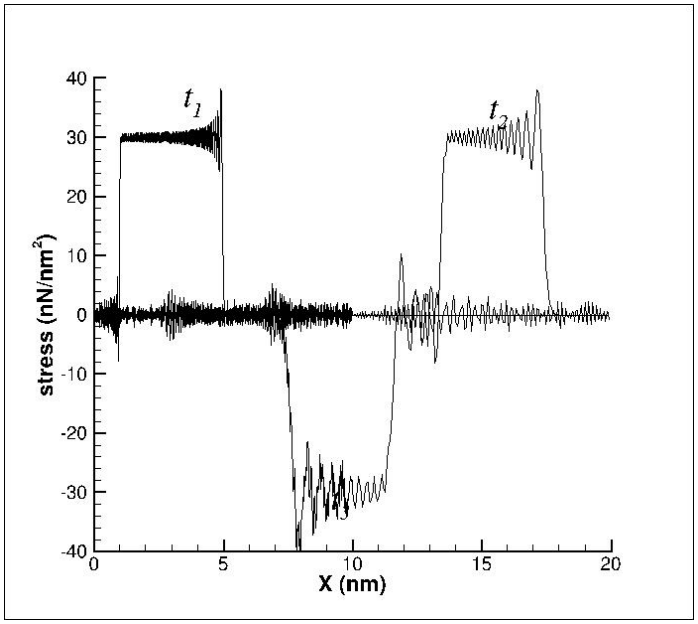

Figure 3-22: Square stress wave propagating along a one-dimensional molecular chain with a multiscale model and a spring potential without FCT applied.

Figures 3-1 and 3-12 that the wave correctly transitions from the MD domain to the FE domain. It can also be seen that at the handshake region, at the midpoint of the molecular chain $X = 10$ nm, that some reflection of the generated oscillations is occurring. This is because the oscillations generated in the MD domain are of a higher frequency than those generated in the FE domain, and the FE domain's element size is large than the MD oscillations. Therefore, because the FE domain cannot hold these oscillations, the handshake point acts a fixed end for the oscillations, and they are reflected back into the MD domain. Figure 3-23 shows the wave with the FCT algorithm applied. It can be seen that the reflected oscillations are picked up as small pulses when the algorithm is used.

Similarly, it can be shown that this is not dependent on the potential function, but only the mismatch in size between the MD bond length and the FE element size. Using the LJ potential, the total force on the handshake node can be written as equation 3.14.

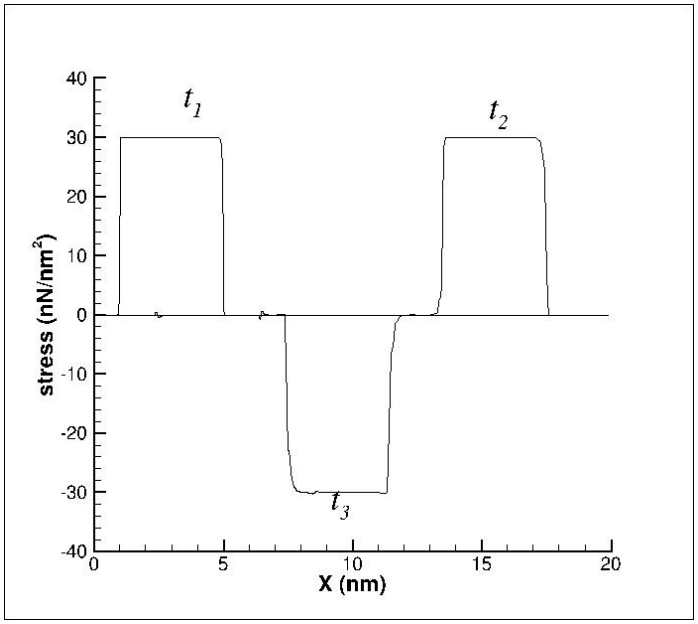

Figure 3-23: Square stress wave propagating along a one-dimensional molecular chain with a multiscale model and a spring potential with FCT applied.

Keeping the parameters the same as in the MD and FE models with $\varepsilon = 10$ nJ, $r_0 = 0.01$ nm, and $l_0 = 0.05$ nm, a force of magnitude 30 nN is applied for 0.004 s and then released. Figures 3-24 and 3-25 show the wave at times $t_1 = 0.0075$, $t_2 = 0.0175$, and $t_3 = 0.035$ s before and after applying the FCT, respectively. It can be seen that while the wave again transitions properly from the MD domain to the FE domain, there are still reflections which get picked up by the FCT algorithm and appear as small pulses. In order to reduce these pulses as much as possible, a transition regime can be used where

Equation 3.14: Total force on handshake particle with LJ potential

$$f_i^{tot} = f_i^{ext} + 12\frac{\varepsilon}{r_0}\left[\left(\frac{r_0}{u_i - u_{i-1}}\right)^7 - \left(\frac{r_0}{u_i - u_{i-1}}\right)^{13} - \left(\frac{l_0}{u_{i+1} - u_i}\right)^7 + \left(\frac{l_0}{u_{i+1} - u_i}\right)^{13}\right]$$

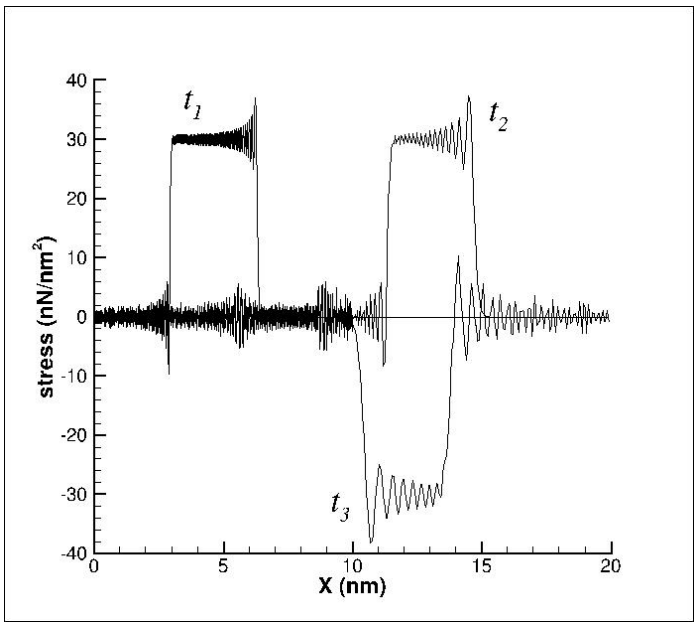

Figure 3-24: Square stress wave propagating along a one-dimensional molecular chain with a multiscale model and a LJ potential without FCT applied.

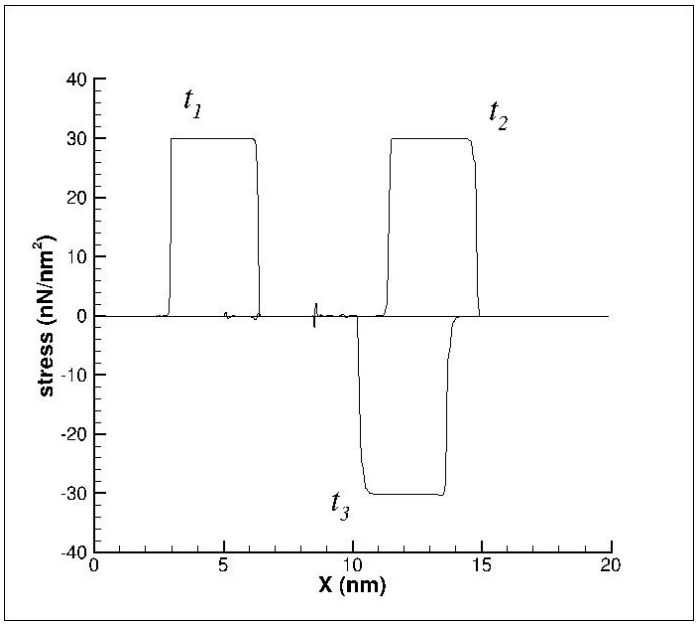

Figure 3-25: Square stress wave propagating along a one-dimensional molecular chain with a multiscale model and a LJ potential with FCT applied.

the FE element size is gradually increased to the full length, rather than immediately start at the full size coming from the MD domain.

This can be done by increasing consecutive element sizes by one bond length until they reach the standard element size, as illustrated in Figure 3-26. In this case, the

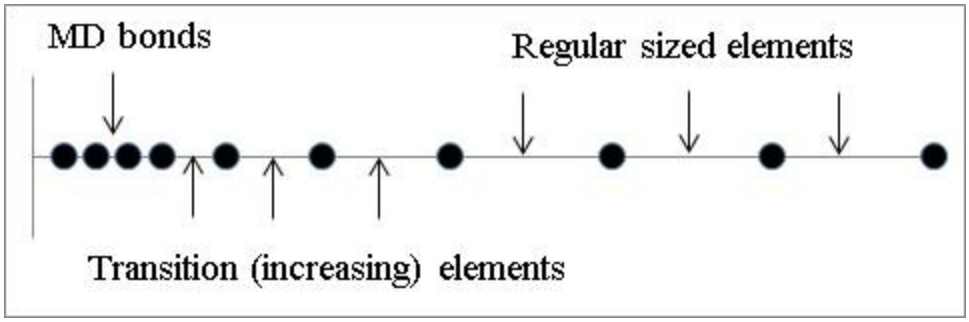

Figure 3-26: Example of transition region elements.

first FE element, connected to the handshake particle, will be two bond lengths, $l_{02} = 2 * r_0$, the next two being three and four bond lengths respectively, $l_{03} = 3 * r_0$ and $l_{04} = 4 * r_0$, and the rest of the elements being the standard five bond lengths long. Equations 3.13 and 3.14 still apply for the handshake particle, with l_0 being replaced with l_{02}, the FE element associated with the handshake region. Using the same spring potential parameters used for Figures 3-22 and 3-23, the square wave is again examined using a multiscale model with the transition region. As seen in Figure 3-27, there are still some oscillation reflections when the FCT algorithm is not used, and there is no observable difference between the multiscale models with and without the transition region. However, it can be seen in Figure 3-28 that when the FCT algorithm is applied, the small pulses are reduced even further than in Figure 3-23, and are nearly completely removed. It is known from the MD and FE models that the square wave and the decaying wave have different oscillations generated. The decaying wave is shown in Figures 3-29 and

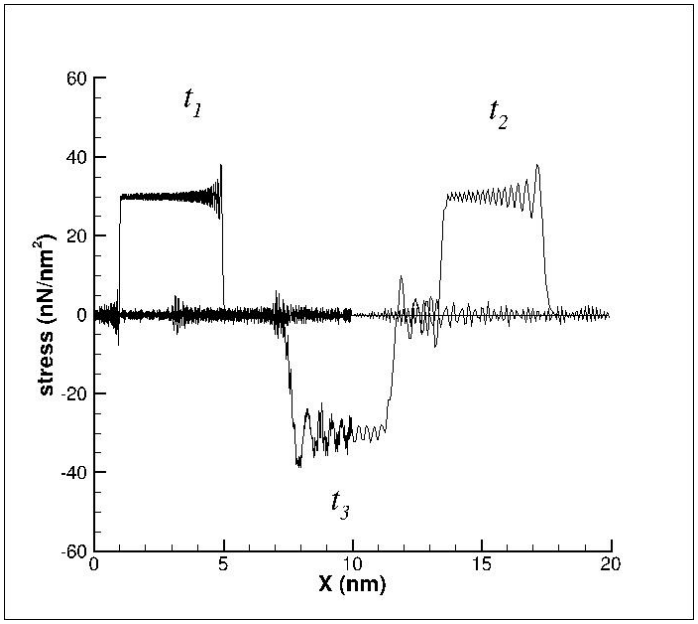

Figure 3-27: Square stress wave propagating along a one-dimensional molecular chain with a multiscale model with a transition region and a spring potential without FCT applied.

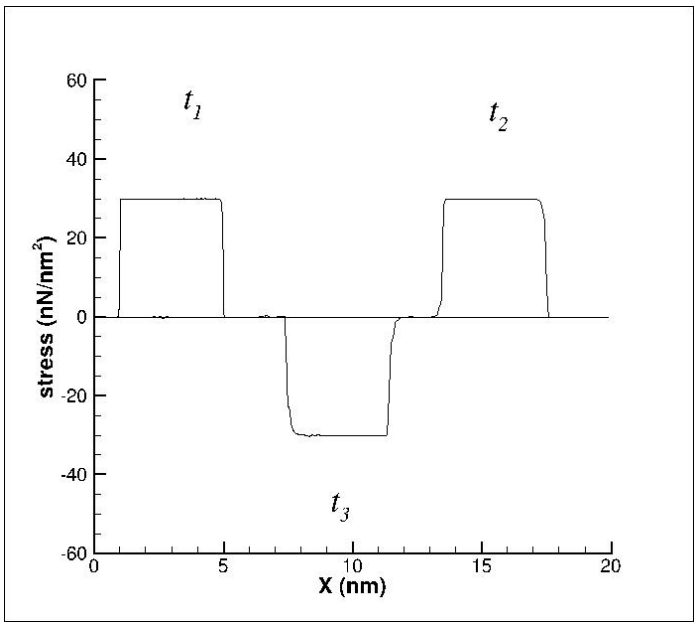

Figure 3-28: Square stress wave propagating along a one-dimensional molecular chain with a multiscale model with a transition region and a spring potential with FCT applied.

3-30 before and after applying the FCT algorithm, respectively. It can be seen in Figure 3-29 that indeed there is a small pulse of oscillations that were reflected, and that in Figure 3-30, the FCT algorithm reduces the pulse to approximately zero.

Next, the multiscale model with a transition region will be investigated for the LJ potential. It can be seen from both the MD models and the FE models that oscillations generated when using the LJ potential are generally greater in magnitude than those generated when using the spring potential and as such it is important to examine each case for the LJ potential in the multiscale model as well. The parameters used are the

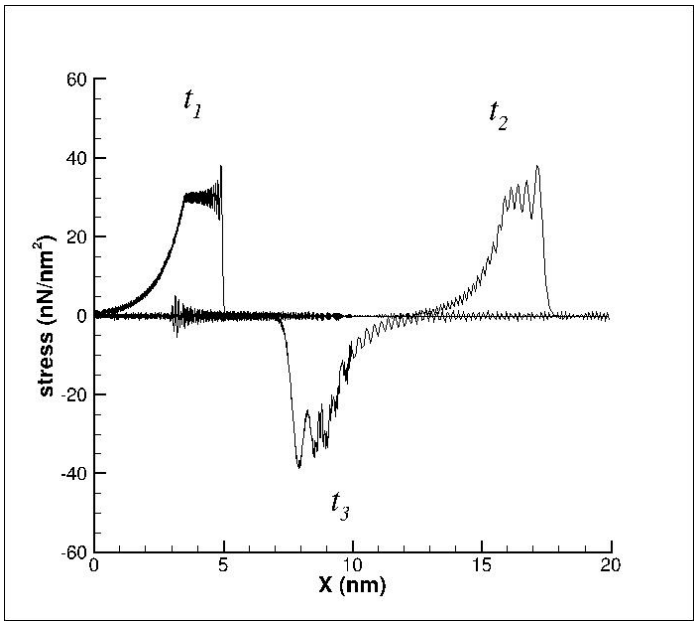

Figure 3-29: Decaying stress wave propagating along a one-dimensional molecular chain with a multiscale model with a transition region and a spring potential without FCT applied.

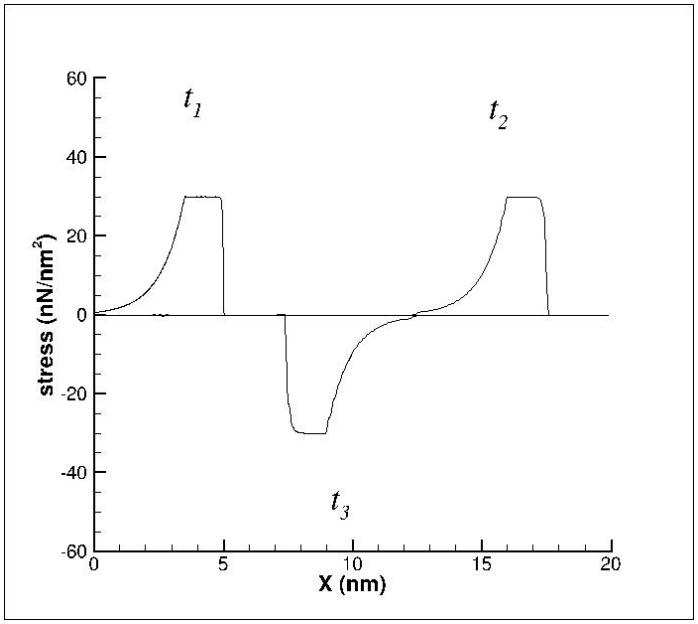

Figure 3-30: Decaying stress wave propagating along a one-dimensional molecular chain with a multiscale model with a transition region and a spring potential with FCT applied.

same as were used in the previous multiscale model, and three elements are again used in the transition region, $l_{02} = 2 * r_0$, $l_{03} = 3 * r_0$, and $l_{04} = 4 * r_0$. In Figures 3-31 and 3-32, the square stress wave is shown before and after the FCT algorithm being applied, respectively. It can be seen that, compared to the MD and FE models, the wave is correctly transitioning from one domain to the other as expected. It can also be seen that the oscillations are indeed reflected at the handshake region, and are of greater magnitude than in Figure 3-27 where the spring potential is used. Figure 3-32 shows that with the transition region, the FCT results in a much smoother result compared to Figure 3-25 where the oscillations are clearly result in small pulses. While the position of these pulses can still be seen in Figure 3-32, they are of negligible magnitude.

It is also known from the MD and FE models that when using the LJ potential, a decaying wave will behave differently in regards to the speed difference between the loading and unloading waves, depending on the initial magnitude of the applied load.

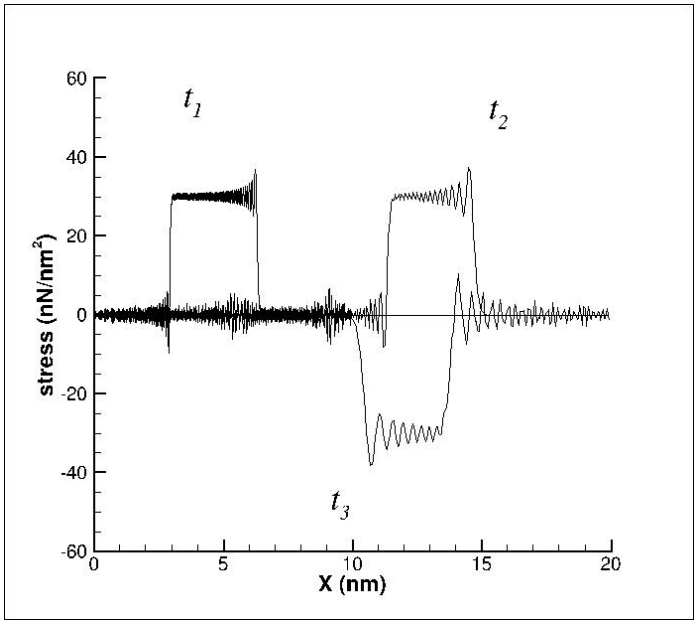

Figure 3-31: Square stress wave propagating along a one-dimensional molecular chain with a multiscale model with a transition region and a LJ potential without FCT applied.

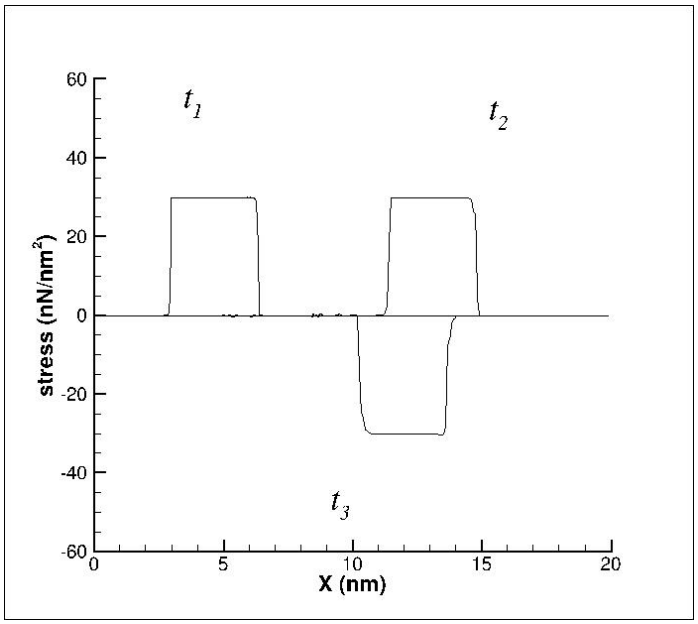

Figure 3-32: Square stress wave propagating along a one-dimensional molecular chain with a multiscale model with a transition region and a LJ potential with FCT applied.

Figures 3-33 and 3-34 show the lower magnitude wave before and after the FCT application, respectively, while Figures 3-35 and 3-36 show the high magnitude wave before and after the FCT application, respectively. It can be seen that the oscillations, and subsequent reflections, in the MD domain appear to be relatively larger for the low magnitude wave than those for the high magnitude wave. However, the oscillations generated in the FE domain are clearly larger, relative to the applied load, for the high magnitude wave. In both cases though, the FCT algorithm effectively removes these oscillations and, with the transition region, not generate the small pulses associated with the reflections.

It has been shown that the FCT algorithm can efficiently remove the oscillations in a multiscale model for both the spring potential and the LJ potential. However, a transition region must be included between the MD domain and the FE domain in order to avoid the generation of small pulses in the MD domain. In the next chapter, a multiscale model can then be used while including another method, which allows for the temperature effects to be included in the simulation.

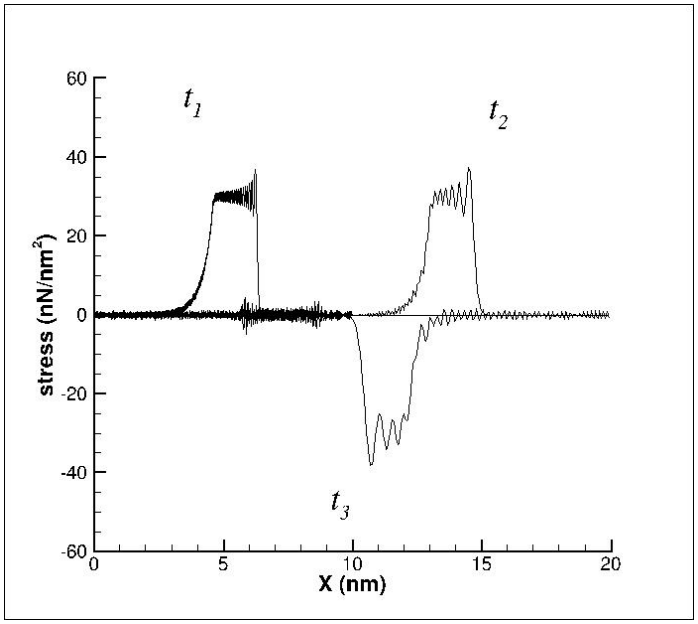

Figure 3-33: Low magnitude decaying stress wave propagating along a one-dimensional molecular chain with a multiscale model with a transition region and a LJ potential without FCT applied.

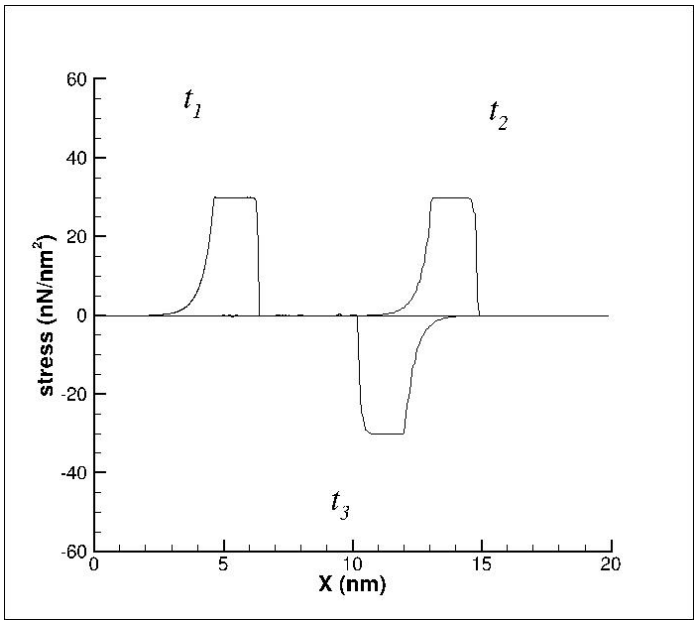

Figure 3-34: Low magnitude decaying stress wave propagating along a one-dimensional molecular chain with a multiscale model with a transition region and a LJ potential with FCT applied.

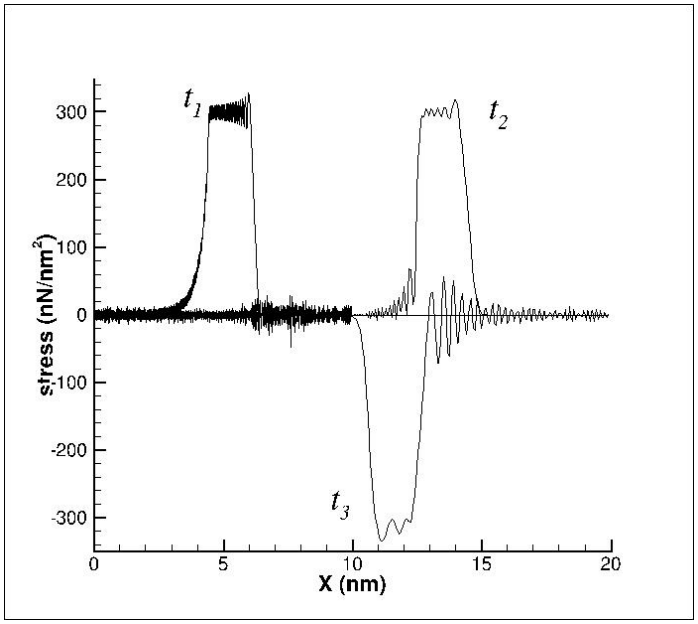

Figure 3-35: High magnitude decaying stress wave propagating along a one-dimensional molecular chain with a multiscale model with a transition region and a LJ potential with FCT applied.

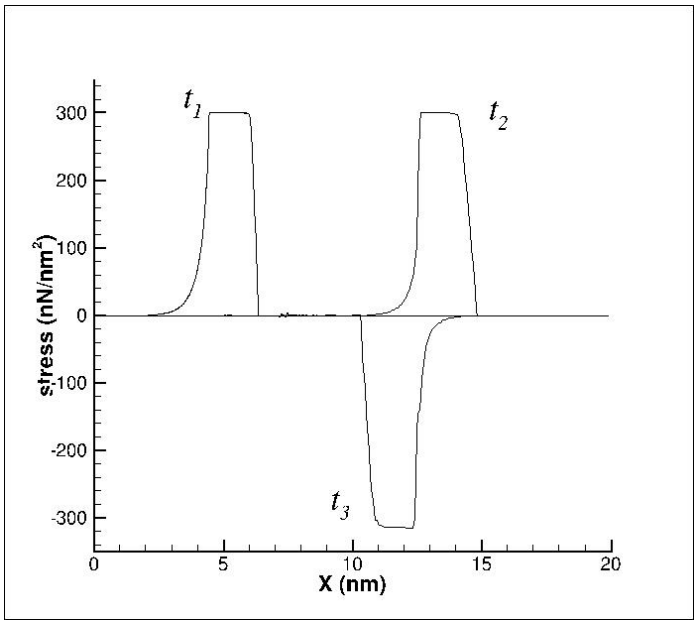

Figure 3-36: High magnitude decaying stress wave propagating along a one-dimensional molecular chain with a multiscale model with a transition region and a LJ potential with FCT applied.

CHAPTER 4

NON-ZERO TEMPERATURE EFFECTS

Traditionally, temperature is included in molecular dynamics simulations by prescribing an increased average velocity across all the atoms with a Boltzmann distribution, which has a mean of zero and standard deviation dependent on desired temperature. This is a problem when it is desired to use the FCT algorithm to improve the accuracy, because the prescribed vibrations are removed by the algorithm. Therefore, it is necessary to find an alternate method for including the temperature effects while applying the FCT to the simulation. This can be done by using the free energy, opposed to the potential energy, of a system and using the Temperature-Related Cauchy-Born Rule (TCB) as a homogenization technique.

4.1 Monte Carlo Simulation

From Equation 2.32, the free energy is still dependent on the potential energy, so the potential function chosen is still an important factor on the system properties. It is clear that the stiffness, from the second derivative of the energy, will be different for the free energy than the potential energy. However, it is also known that with increased temperature, most materials expand, so that the undeformed bonds will have different values than the zero temperature case (potential energy only). To determine the new undeformed bond lengths, a Monte Carlo simulation can be done using the free energy. Then, new parameters for a new approximation potential can be found with the new bond length and free energy at that point.

First, a potential function must be chosen. In this case, the LJ potential will again be examined, but not the spring potential. This is because in equations 2.32 and 2.33, the diagonalized matrix **D**, for a one dimensional system, is the second derivative of the potential. In the case of the spring potential, the second derivative is a constant, so when the stress is calculated by taking the derivative, this becomes zero, and only the potential

term remains. Also, it is important to note that parameter choices must be more careful, because if the potential chosen is too stiff, then the potential dominates the temperature term, and the temperature effects become negligible. Conversely, if the chosen potential is not stiff enough, the bonds will break too easily when the temperature is included, and the system will become unstable. From these limits, the parameters for the LJ potential are $\varepsilon = 15.0 * 10^{-19}$ J and $r_0 = 1.0$ nm, arbitrary values.

Using equation 2.19, the new bond lengths are found by incrementally increasing the volume, and comparing the resulting free energy densities. Figure 4-1 shows the results for the MC simulation when the temperature is set to the average room temperature of 300 K. It can be seen that the minimum energy of $-15.0 * 10^{-19}$ J for the potential is decreased noticeably to approximately $-16.2 * 10^{-19}$ J for the free energy. Also, it can be seen that while the equilibrium bond length is increasing, it is much less noticeable, increasing from 1 nm to approximately 1.0004 nm. These values can then be

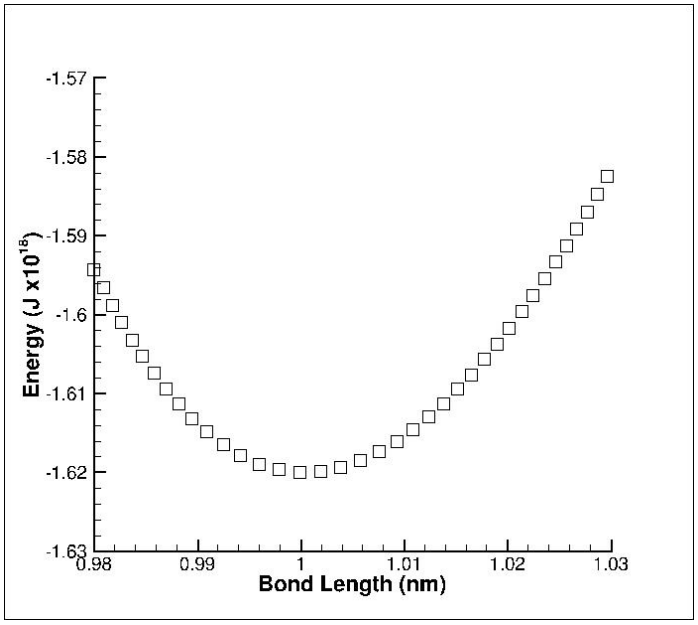

Figure 4-1: MC free energy results for T = 300 K.

used to derive an equivalent potential function for a temperature of 300 K. However, because this will ensure the approximation is equivalent to the free energy only at the equilibrium length, the energy well must be altered slightly so as to make the approximation at increased strain levels also equivalent to the free energy. This can be done by finding an energy depth value that makes the rate of change of the internal force (the second derivative of the potential) as close as possible. In the case of a temperature of 300 K, the new approximation value ε_{300} is approximately 92% of the free energy depth, as shown in equation 4.1, where $\varepsilon_{300} = 14.87 * 10^{-19}$ J and $r_{300} = 1.0004$ nm. The derived potential can then be brought back up to the free energy level by adding the difference as a constant, as shown in equation 4.1. Figure 4-2 shows a comparison between the free energy, the derived potential which only matches the energy depth, and the derived potential which matches the energy depth as well as the gradient. It can be seen that the adjustment to match the gradient increases the accuracy of the derived potential function. Figure 4-3 shows a comparison between the gradients (internal forces) of the free energy and equation 4.1 around the equilibrium bond length up to strain levels of 5%, and shows that it is a good approximation for the free energy as long as the bond lengths do not expand or contract too much. This process can be repeated for any desired temperature.

As a comparison, Figure 4-4 shows the MC results for T = 200 K. Therefore, the parameters for the equivalent potential are $\varepsilon_{200} = 14.50 * 10^{-19}$ J and $r_{200} = 1.0003$ nm. Figure 4-5 shows a comparison between the results for T = 200 K and T = 300 K. It can be seen that as expected, the energy well continues to decrease with an increase in temperature. A comparison of the free energy and derived potential at T = 200 K can be

Equation 4.1: Potential equivalent for T = 300 K

$$U_{300} = 4\varepsilon_{300}\left[\frac{1}{4}\left(\frac{r_{300}}{r}\right)^{12} - \frac{1}{2}\left(\frac{r_{300}}{r}\right)^{6}\right] - 1.32 * 10^{-19}$$

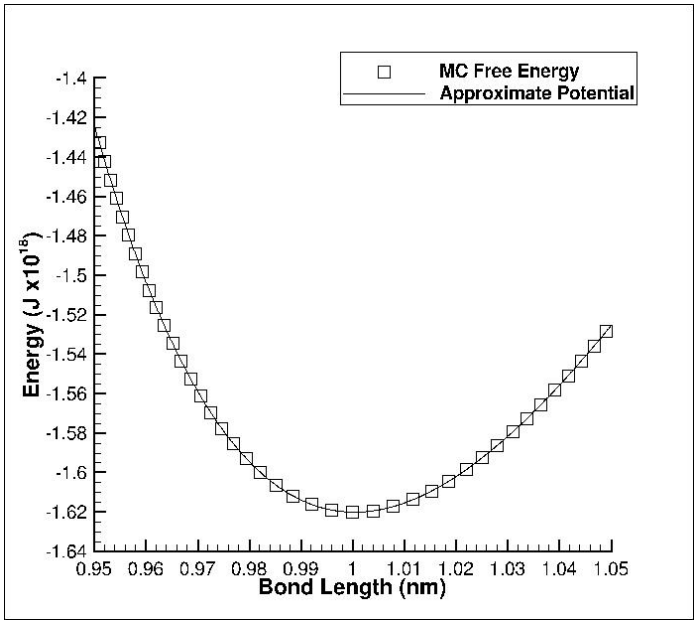

Figure 4-2: Comparison of free energy from MC simulation and derived potential functions at 300 K.

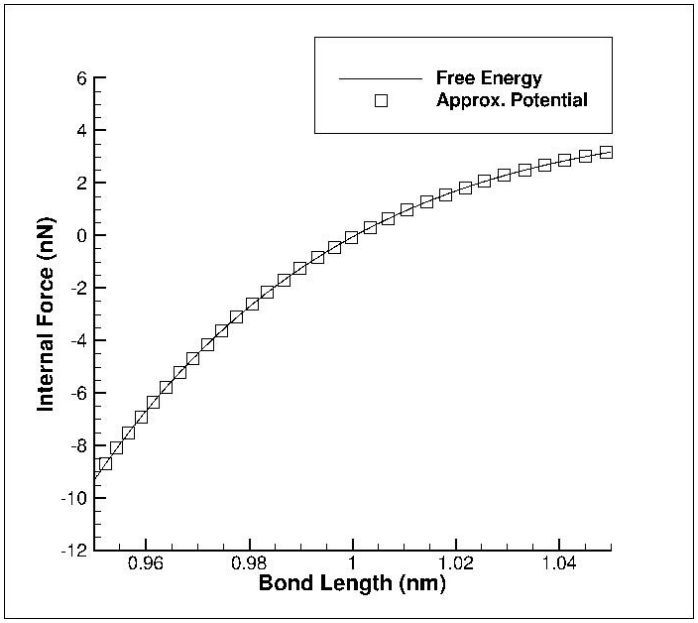

Figure 4-3: Comparison of free energy from MC simulation and approximation potential gradients at 300 K.

seen in Figure 4-6. It can be seen that for the case where the temperature is set at 200 K, adjusting the potential to match the gradient of the free energy produces a larger increase in accuracy than for the previous case. Figure 4-7 shows the comparison between the gradients of the free energy and the equivalent potential function for T = 200 K. It is important that the approximation potentials are representative of the free energy as much as possible, because if there is a noticeable difference, the MD and FE domains will essentially be composed of different materials. This would cause reflections of the wave at the interface which is due to material properties, not numerical errors.

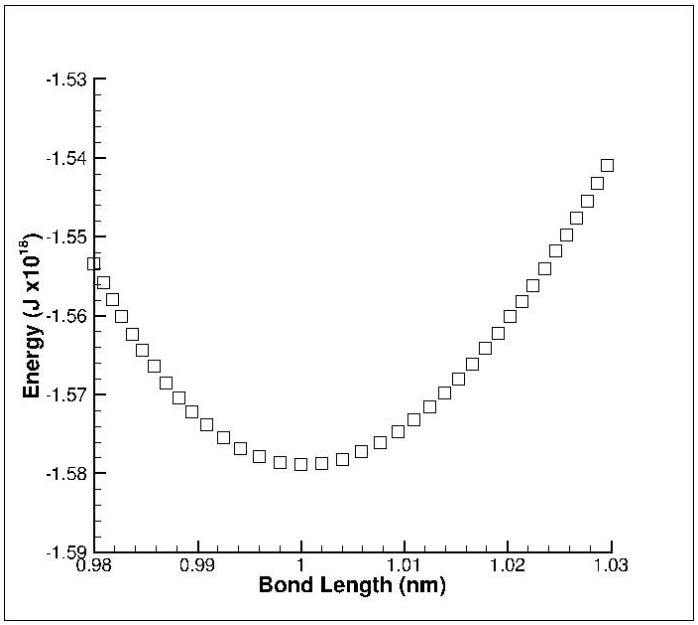

Figure 4-4: MC free energy results for T = 200 K.

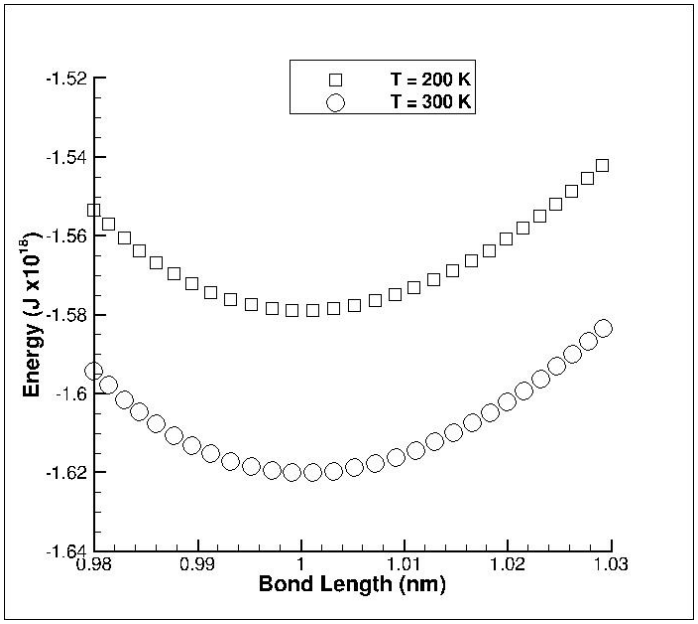

Figure 4-5: Comparison of free energy from MC simulations at different temperatures.

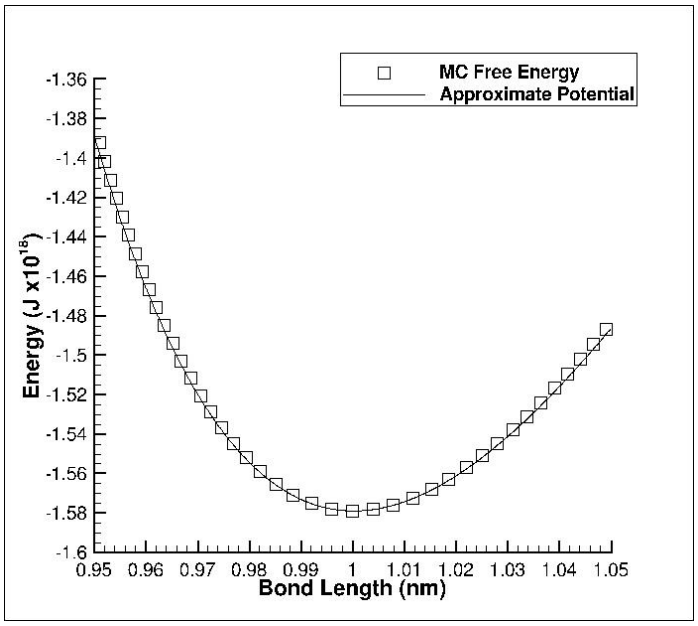

Figure 4-6: Comparison of free energy from MC simulation and derived potential functions at 200 K.

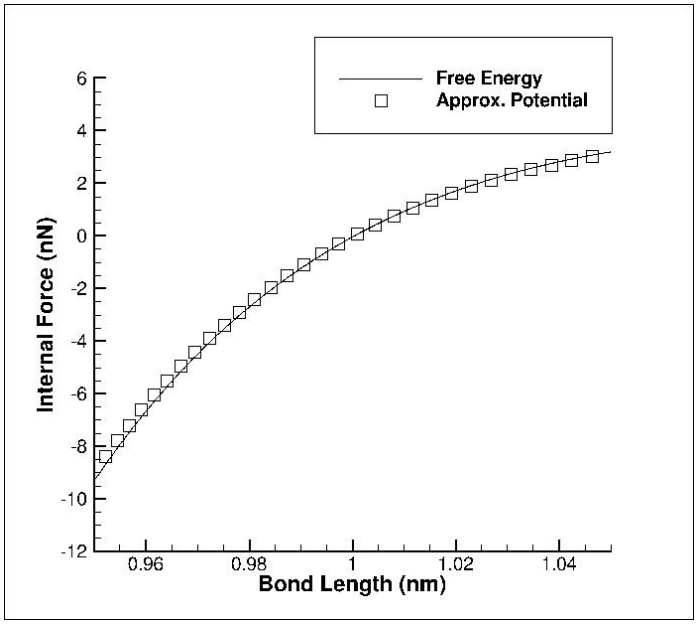

Figure 4-7: Comparison of free energy from MC simulation and approximation potential gradients at 200 K.

4.2 Shockwave Propagation with TCB Rule

For the FE domains, the Temperature-Related Cauchy-Born Rule will be used to incorporate the effects from the prescribed temperature. Because the system is one-dimensional, the degrees of freedom *n* in equation 2.37 is one. The TCB rule for the free energy can then be written as equation 4.2. The PK stress can then be found by taking the derivative of equation 4.2 with respect to *r* from equation 2.39. Using the LJ potential function, the PK stress can be written in semi-simplified form as equation 4.3. It should noted that in equations 4.2 and 4.3, the potential U, and parameters ε and r_0, are from the

Equation 4.2: TCB rule free energy homogenization

$$F_H = U + k_b T \ln\left[\frac{2\bar{h}\sqrt{\frac{d^2U}{dr^2}}}{k_b T}\right]$$

Equation 4.3: TCB rule PK stress

$$\mathbf{P} = \frac{12\varepsilon}{r_0}\left[\frac{1}{\mathbf{F}^7} - \frac{1}{\mathbf{F}^{13}}\right] + \frac{k_b T}{r_0}\left[\frac{\left(\frac{4}{\mathbf{F}} - \frac{13}{\mathbf{F}^7}\right)}{\left(\frac{13}{7\mathbf{F}^6} - 1\right)}\right]$$

original LJ potential function, not the derived approximations. This is because the second term is used to alter the potential energy relative to the temperature.

Using the same parameters chosen for the MC simulations, $\varepsilon = 15.0 * 10^{-19}$ J and $r_0 = 1.0$ nm, a shockwave can be simulated using a multiscale model with FE element size $l_0 = 5.0$ nm. The transition region will be in the center of the model, as studied in the previous chapter, and the molecular chain will have a length of 2000 total bond lengths, or 2.0 μm. The MD domain will be governed by the derived approximate potentials as in equation 4.1, while the FE domain will be governed by the TCB rule, equations 4.2 and 4.3. Figure 4-8 shows a comparison of a wave propagating with the

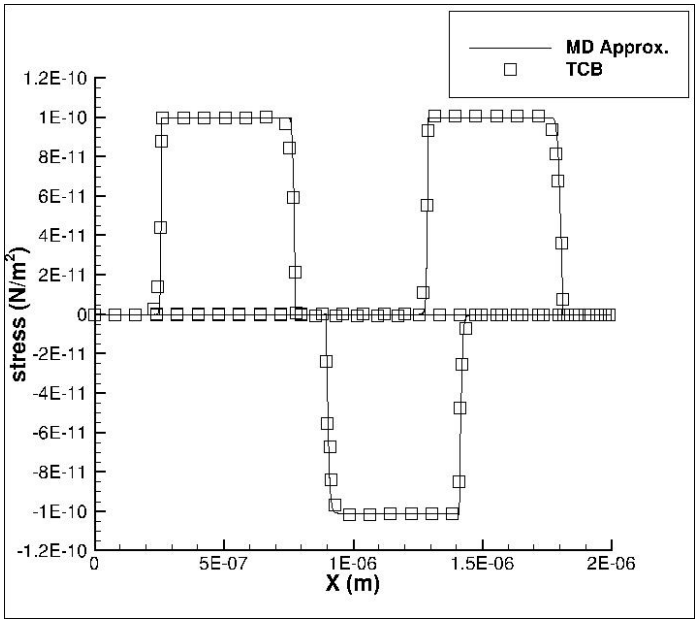

Figure 4-8: Comparison of wave propagation with TCB and derived potential.

TCB in a FE-only model and a MD-only model with the derived approximation potential. It can be seen that the two have a very good relationship, so the multiscale model can be used. Two wave shapes will be tested: the square wave with constant magnitude and the exponentially decaying wave with an initial magnitude that decreases exponentially after a given time. A force with an initial magnitude of 10 nN will be applied to the end of the molecular chain. As a reference case, the zero temperature case will be examined first.

First, the square wave will be examined. The force is applied for 0.5 ms, and then released. Figure 4-9 shows the wave at times $t_1 = 0.75$, $t_2 = 1.75$ and $t_3 = 3.0$ ms without the FCT algorithm. Figure 4-9 shows the wave with the FCT algorithm, with a very good discontinuous shock front, no oscillations, and no pulses due to reflection. This agrees with the results found in the previous chapter, as only the potential is considered when the temperature is set to zero. Figures 4-10 and 4-11 show the decaying wave

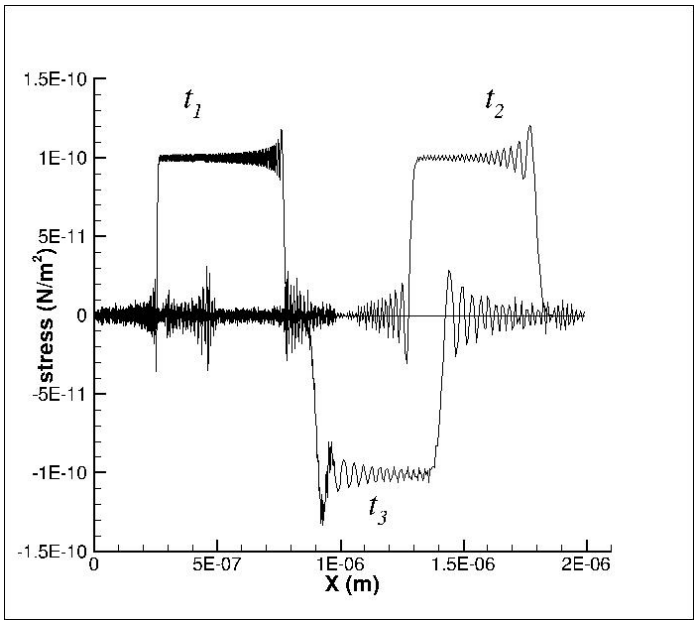

Figure 4-9: Square stress wave at zero temperature without FCT.

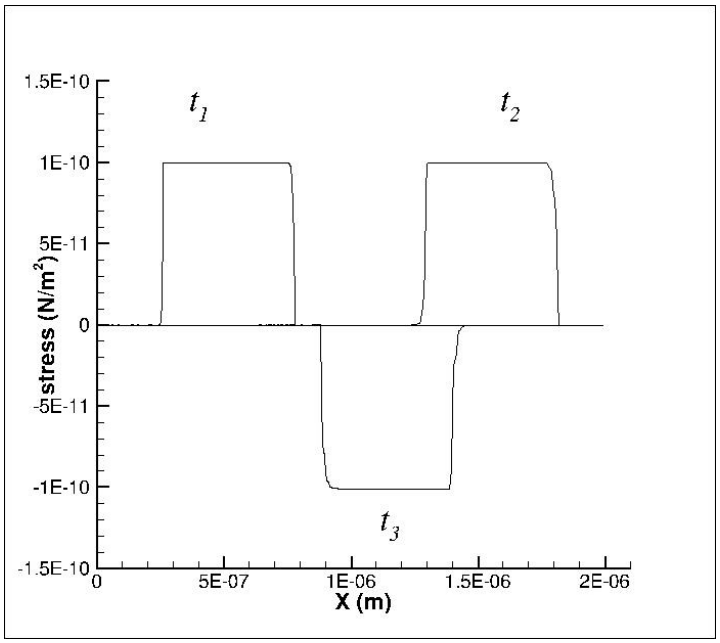

Figure 4-10: Square stress wave at zero temperature with FCT.

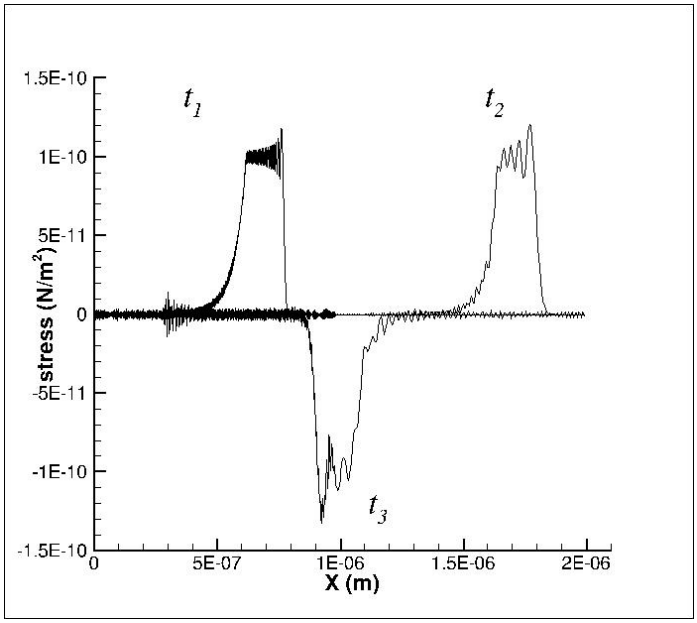

Figure 4-11: Decaying stress wave at zero temperature without FCT.

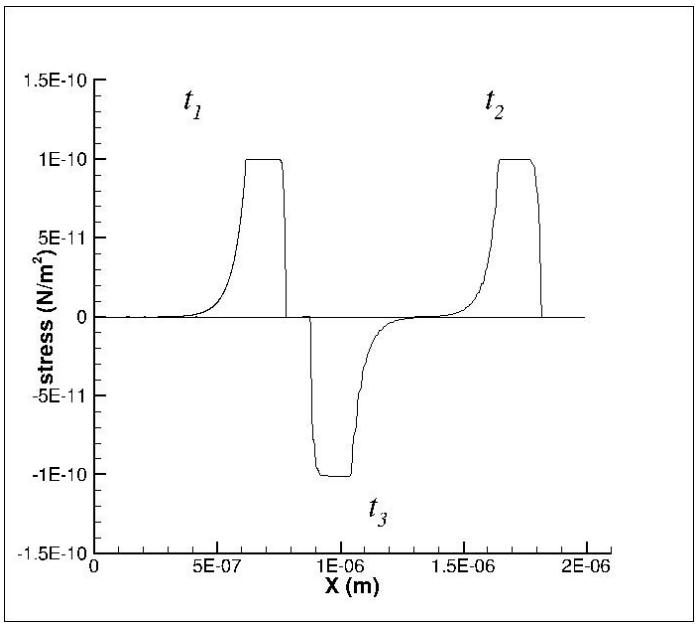

Figure 4-12: Decaying stress wave at zero temperature with FCT.

before and after applying the FCT algorithm, respectively. The initial magnitude was held for 0.15 ms, and then decreased exponentially down to zero. Because the LJ potential is used, the effects due to the difference in speed between the loading wave and the unloading wave can be seen. Again the FCT algorithm provides a very good discontinuous shock front without oscillations or the pulses due to reflections as expected.

Next, the case when the temperature is set to room temperature, 300 K, will be examined. As previously mentioned, the parameters for the MD domain's potential equivalent are $\varepsilon_{300} = 14.87 * 10^{-19}$ J and $r_{300} = 1.0004$ nm. Figures 4-13 and 4-14 show the square wave before and after the application of the FCT algorithm, respectively, while Figures 4-15 and 4-16 show the decaying wave. It can be seen that there are very small reflections due to the small differences between the approximation potential and free energy. However, they are similar enough that the reflections are negligible

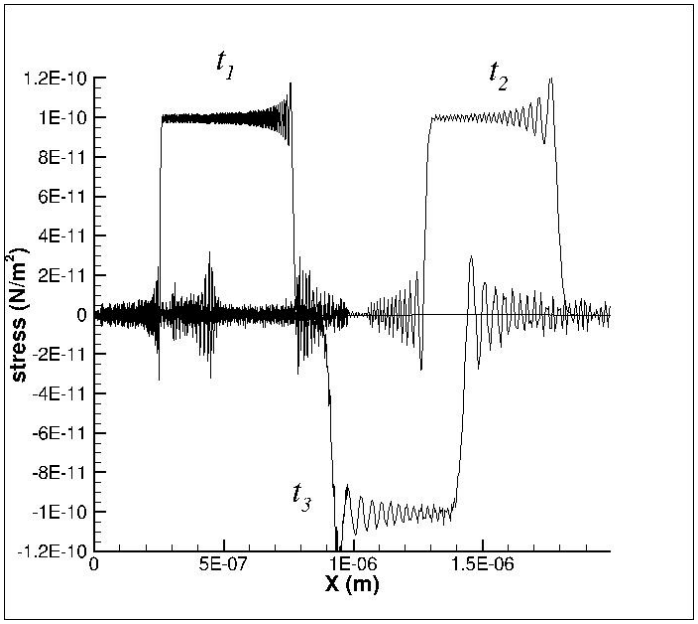

Figure 4-13: Square stress wave at 300 K without FCT.

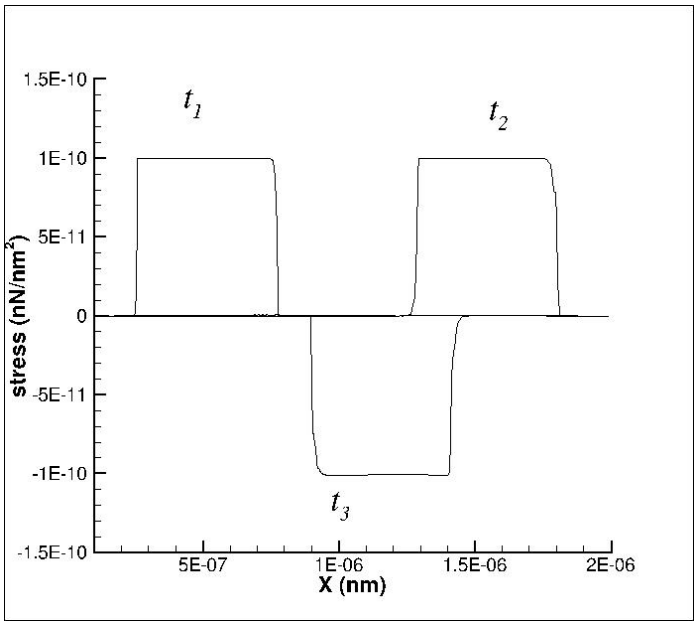

Figure 4-14: Square stress wave at 300 K with FCT.

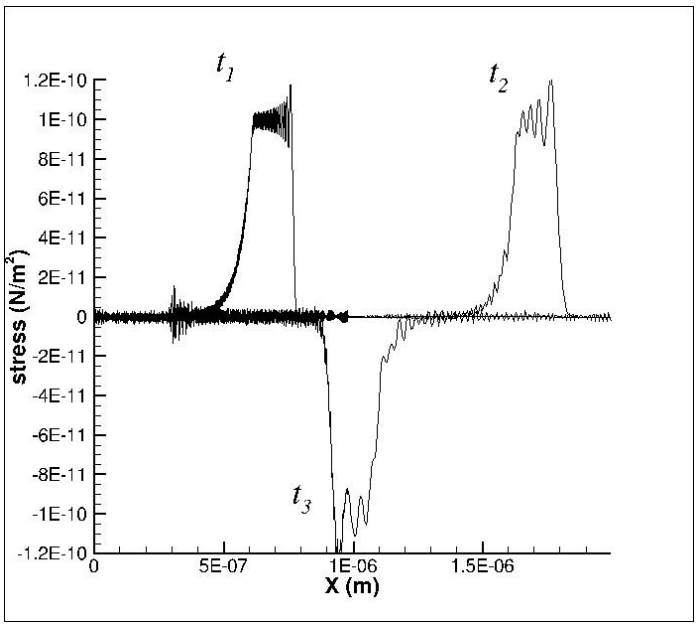

Figure 4-15: Decaying stress wave at 300 K without FCT.

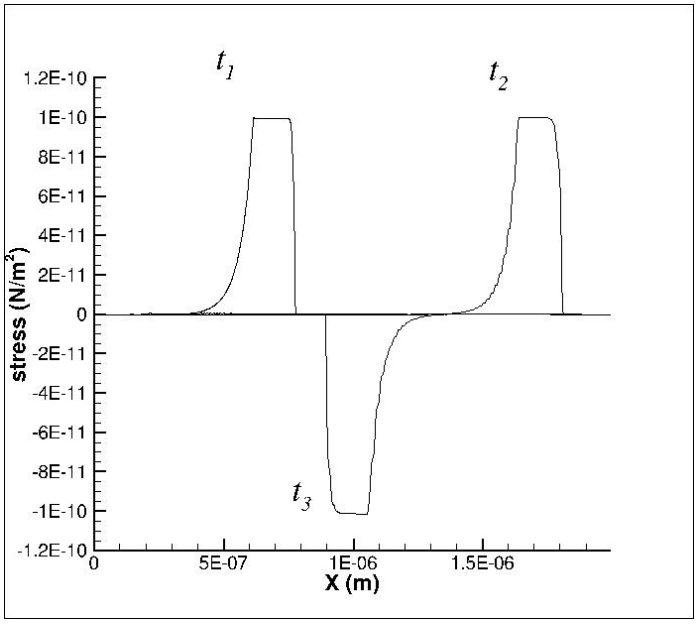

Figure 4-16: Decaying stress wave at 300 K with FCT.

compared to the stress. Figure 4-17 shows a comparison for the cases T = 0 K and T = 300 K. Because higher temperatures correspond to higher molecular kinetic energies, it is expected that the shock waves will travel faster with higher temperature, and Figure 4-17 shows this does indeed occur, although not at a very significant level due to the initial parameters chosen. The larger the discrepancy, the more energy is reflected due to it being the equivalent of having different materials. These figures also show that by using the free energy and the TCB rule, the temperature effects can be included without the use of molecular kinetic energy. The waves clearly retain their shape and size from the zero temperature, where only the original potential function is used, to the higher temperatures. Figures 4-18 through 4-21 show the wave for the case when T = 200 K. While the temperatures are close enough that the wave speed difference is not noticeable, it can be seen the capability of the free energy method and FCT is viable for any temperature, assuming that the bonds do not break due to the temperature.

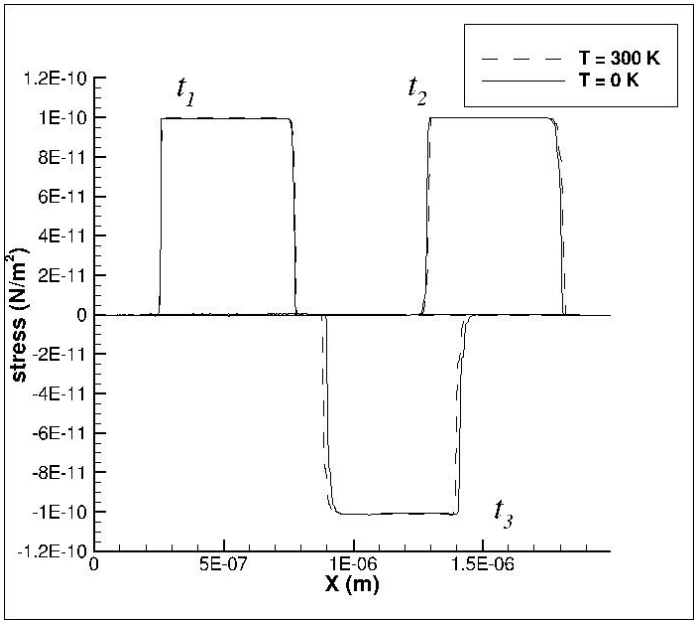

Figure 4-17: Wave speed comparison for temperatures of 0 K and 300 K.

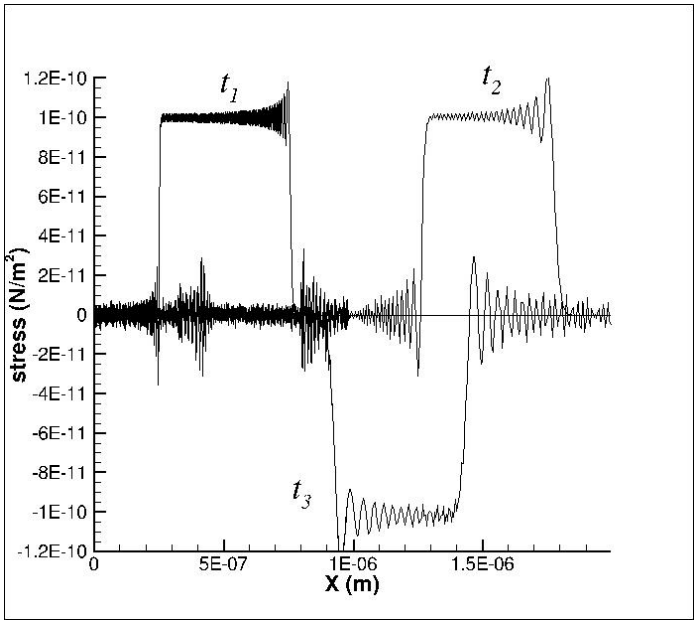

Figure 4-18: Square stress wave at 200 K without FCT.

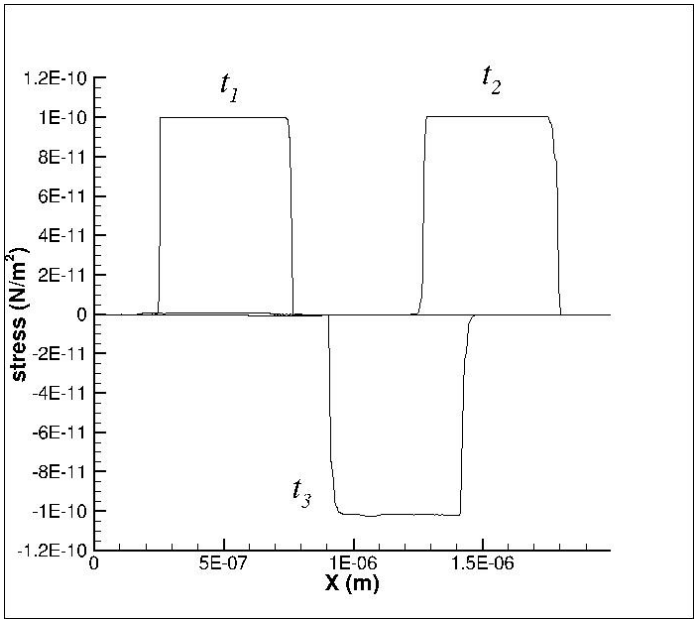

Figure 4-19: Square stress wave at 200 K with FCT.

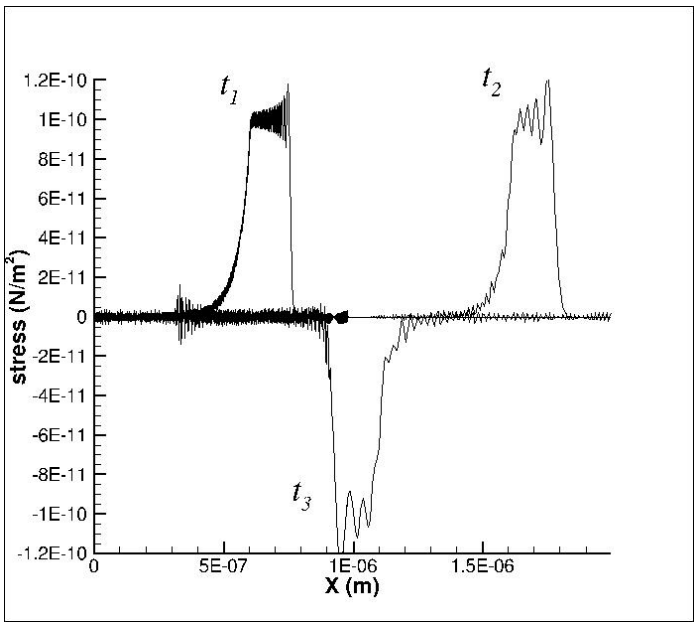

Figure 4-20: Decaying stress wave at 200 K without FCT.

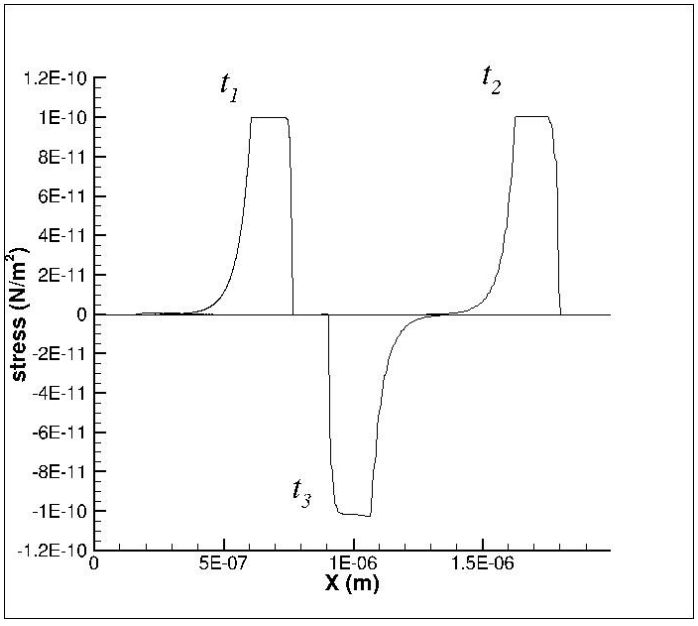

Figure 4-21: Decaying stress wave at 200 K with FCT.

CHAPTER 5

SUMMARY AND RECOMMENDATONS

5.1 Summary and Conclusions

In this thesis the simulation of shockwave propagation in a one-dimensional solid was studied. The simulations were investigated using multiscale models, to compare the effects from the molecular scale to the continuum scale. The removal of oscillations behind the shock fronts, which were generated as numerical errors, was also investigated using the finite element flux-corrected transport algorithms. Lastly, a method to study the temperature effects without using velocity scaling was investigated by utilizing the free energy and the Temperature-Related Cauchy-Born Rule.

The multiscale modeling was done by coupling the molecular dynamics from the molecular domain to the finite element analysis from the continuum domain by using the edge to edge Macroscopic Atomistic *Ab Initio* Dynamics method. It was found that as the element size to bond length ratio increased at the MAAD edge, there was greater reflections of the oscillations generated in the MD domain. As a result, when the FCT algorithm was applied these reflections produced small pulses in the model, which were nonphysical results. It was found that a transition region from MD to FE domain was needed to remove these pulses, by gradually increasing the element size of the continuum domain from very close to the MD bond length (less than double) up to the regular element size used for most of the FE model. The smaller the incremental increase in element size, the more the reflections were reduced. It was found that the pulses became negligible by using an increment size of one fourth of the original bond length, although this can differ based on the material properties. Once the transition region was established, the FCT was able to effectively remove the numerical errors while keeping a sharp, discontinuous wave front for a variety wave shapes, including shapes which typically began breaking down due to the errors when the FCT had not been applied.

While multiscale models can overcome the time and length scale limits of Molecular Dynamics, the temperature effects are still difficult to study. By utilizing the free energy and TCB rule, the temperature effects on the shockwave propagation were able to be approximated. This was done by first using a Monte Carlo simulation to obtain a plot of the free energy, which is dependent on the temperature. Using the data from the MC simulation, a new potential function was derived for the MD domain, while the FE domain was homogenized by the TCB rule, which also utilizes the free energy to capture the temperature effects. Using these two methods, various effects due to temperature were able to be captured, such as the deepening of the energy well, an increase in the undeformed bond length, and an increase in wave speed. As expected, it was found that if the molecular bonds were too stiff that the temperature effects became negligible and there was little difference from the zero temperature case. Similarly, if the bonds were too soft, the temperature effects caused the bonds to break and the model became unstable. Because of this, if the potential function is biased towards one extreme or the other, then the new potential approximation that was derived for a certain temperature will diverge from the free energy as the bond length differs from undeformed length. Because the TCB rule in the FE domain is always governed by the free energy, this divergence can cause the MD domain and FE domain to effectively behave as different materials, and create energy reflections at the multiscale coupling interface. Because these reflections are due to apparent differences in material properties and not numerical error, the transition region will do little to eliminate these reflections. Only a closer approximation between the new molecular potential and the free energy will effectively reduce these reflections.

5.2 Future Work

Several recommendations can be made for the further study of shockwave propagation in multiscale models and non-zero temperature fields. It is known that if the

molecular bonds are stretched too far, the bonds will break, releasing energy. This released energy can be incorporated as an increase in local temperature. The effects of this non-homogenous temperature field can be studied by including a thermo-mechanical coupling based on this increase in local temperature. The temperature gradient can be studied by using the thermal diffusion equations along with the TCB rule. The multiscale effects can also be improved by using a more robust multiscale coupling method. For example, the Bridging Domain Coupling Method imposes constraints to extend the coupling region from a single edge to a separate region, where both the MD and FE regions simultaneously govern the motion.

Also, the simulations were done using fictitious materials with arbitrary properties. This was done primarily for verification of the proposed methods. The methods used can easily be extended for use with realistic material properties and practical problems. As such, further research can obtain experimental data to evaluate the simulation results.

REFERENCES

Boris, Jay P., Book, David L. 1973. “Flux-Corrected Transport.” Journal of Computational Physics 11:38-69.

Davison, Lee. 2008. *Fundamentals of Shockwave Propagation in Solids.* Berlin, Heidelberg : Springer-Verlag Berlin Heidelberg, 2008.

Dupuy, L. M., Tadmor, E. B., Miller, R. E., Phillips, R. 2005. “Finite Temperature Quasicontinuum: Molecular Dynamics without All the Atoms.” Physical Review Letters 95, 060202.

E, Weinan, Engquist, Bjorn. 2003. “Multiscale Modeling and Computation.” Notices of the AMS 50:1062-1070.

E, Weinan, Ming, Pingbing. 2006. “Cauchy-Born Rule and the Stability of Crystalline Solids: Static Problems.” Archive for Rational Mechanics and Analysis 183:241-297.

E, Weinan. 2011. *Principles of Multiscale Modeling.* Cambridge : Cambridge University Press, 2011.

Frenkel, Daan, Smit, Berend. 1996. *Understanding Molecular Simulations.* California : Elsevier, 1996.

Hilber, Hans M., Hughes, Thomas J. R., Taylor, Robert L. 1977. “Improved Numerical Dissipation for Time Integration Algorithms in Structural Dynamics.” Earthquake Engineering and Structural Dynamics 5:283-292.

Kawai, S., Lele S. K. 2007. “Localized artificial viscosity and diffusivity scheme for capturing discontinuities on curvilinear and anisotropic meshes.” Center for Turbulence Research : Annual Research Briefs 2007.

Lu, Gang, Kaxiras, Efthimios. 2005. *Handbook of Theoretical and Computational Nanotechnology.* Volume X:1-33.

Mariani, Steffano, Martini, Roberto, Ghisi, Aldo. 2009. “A Finite Element Flux-Corrected Transport Method for Wave Propagation in Heterogeneous Solids.” Algorithms 2009 2:1-18.

Najafabadi, R., Srolovitz, D.J. 1992. “Order-disorder transitions at and segregation to (001) Ni-Pt surfaces.” Surface Science 286:104-115

Xiao, S.P. 2004. “An FE-FCT method with implicit functions for the study of shock wave propagation in solids.” *Wave Motion* 40:263-276.

Xiao, S.P., Yang, W. 2006. “A temperature-related homogenization technique and its implementation in the meshfree particle method for nanoscale simulations.” International Journal for Numerical Methods in Engineering 69:2099–2125.